J. Fluid Mech. (2005), *vol.* 541, *pp.* 115–142. © 2005 Cambridge University Press
doi:10.1017/S0022112005005860 Printed in the United Kingdom

The effects of insoluble surfactants on the linear stability of a core–annular flow

By HSIEN-HUNG WEI[1] AND DAVID S. RUMSCHITZKI[2]†

[1]Department of Chemical Engineering, National Cheng Kung University, Tainan, 701, Taiwan
[2]Department of Chemical Engineering and Levich Institute, The City College and GSUC of CUNY, New York, NY 10031, USA

(Received 12 March 2004 and in revised form 26 April 2005)

The effects of an insoluble surfactant on the linear stability of a two-fluid core–annular flow in the thin annulus limit, for axisymmetric disturbances with wavelengths large compared to the annulus thickness, h_0, are the focus of this investigation. A base shear flow affects the interfacial surfactant distribution, thereby inducing Marangoni forces that, along with capillary forces, affect the fluid–fluid interface stability. The resulting system's stability differs markedly from that of the same system with zero base flow. In the thin-annulus limit (the ratio ε of the undisturbed annulus thickness to core radius tends to zero), common in applications, a scaling and asymptotic analysis yields a coupled set of equations for the perturbed fluid–fluid interface shape and surfactant concentration. The linear dynamics of the annular film fully determine these equations, i.e. the core dynamics are slaved to the film dynamics. The theory provides a unified view of the mechanism of stability in three different regimes of capillary number Ca (defined as the product of the core viscosity, μ_1, and the centreline velocity, W_0, divided by the interface tension, σ_0^*, that corresponds to an undisturbed (signified by the subscript 0) uniform surfactant concentration, Γ_0^*). In the absence of a base flow or in the limit of small $Ca(\ll\varepsilon^2)$, Marangoni forces deriving from non-uniformities in the interface concentration of insoluble surfactants oppose the net capillary forces. These latter forces normally stabilize the longitudinal curvature and destabilize the circumferential curvature of perturbations to the interface. In the limit of large $Ca(\gg\varepsilon^2)$, Marangoni forces destabilize disturbances with wavelengths that are large compared to the annulus thickness. For moderately small $Ca(\sim\varepsilon^2)$, increasing the Marangoni number Ma (defined as the product of $(-\partial\sigma^*/\partial\Gamma^*)_0$ and Γ_0^*, divided by $\mu_1 W_0$) from zero increases the growth rates of all disturbances (with wavelengths $\gg h_0$) and, consequently, reduces the marginal wavelength below that typical of the capillary instability. However a further increase in Ma eventually reverses these trends. A very large value for Ma stiffens the interface, which opposes any local variation of the tangential velocity along the interface, and this is true whether or not there is a base flow. In the limit of infinite Ma, the growth rate of the instability is 1/4 of that of the clean interface and the marginal wavenumber, non-dimensionalized by the undisturbed core circumference, returns to its clean interface (capillary) value of 1. All trends are explained physically.

1. Introduction

A two-fluid core–annular flow (CAF) consists of two immiscible fluids flowing concurrently in a cylindrical tube. This flow system is often employed as a model

† Author to whom correspondence should be addressed.

in technologically important processes, for example, in lubricated pipelines (Preziosi, Chen & Joseph 1989), liquid–liquid displacements in porous media (Park & Homsy 1984), secondary oil recovery (Slattery 1974) and pulmonary fluid mechanics (Otis *et al.* 1993). It is important to understand the mechanism of instability in a CAF because it is often critical in applications to either encourage or discourage this instability.

The dominant terms in the equations that govern the linear stability of a CAF derive from two sources: (i) the perturbation pressure in the annulus caused by capillary forces deriving from the interface perturbation, and (ii) the velocity perturbation at the perturbed interface that results from the different radial derivatives of the base flow axial velocity at the interface when the two fluids have different viscosities. The former source, when present alone, is called the capillary instability and the latter is commonly called 'viscosity stratification' in the literature. The capillary instability has been widely studied for a variety of different arrangements of fluids, all having a cylindrical fluid–fluid interface (Rayleigh 1879; Tomokita 1935; Goren 1962). Capillarity acts in two ways: it destabilizes the interface circumferential curvature and stabilizes the axial curvature. The competition is such that disturbances with wavelengths longer than the undisturbed interfacial circumference are unstable and those with wavelengths shorter are stable. These net destabilizing capillary forces occur (but do not necessarily predominate) irrespective of whether there is a base flow, and arise simply from the cylindrical geometry of the undisturbed fluid–fluid interface. Hickox (1971) found that viscosity stratification could, by itself, linearly destabilize a cylindrical fluid–fluid interface when the more viscous fluid is in the annulus, and that axisymmetric modes are the most dangerous. Preziosi *et al.* (1989) investigated the linear stability of the opposite arrangement (where the ratio m of the annulus to the core fluid viscosities is less than unity), with emphasis on capillarity and viscosity stratification, which is relevant to lubricated pipelines. They numerically solved the full Orr–Sommerfeld equations to show that the viscosity stratification contribution is stabilizing for $m < 1$ and, at large enough Reynolds number, can exceed the destabilizing (to long waves) capillary forces. The net result is a band of Reynolds numbers for which the interface is stable to disturbances of all wavelengths. In most applications, the unperturbed annulus is much thinner than the tube radius; this motivated Georgiou *et al.* (1992) to develop thin film asymptotics to examine analytically the linear stability of a CAF in a vertical arrangement with gravity. Their asymptotic treatment clearly shows that the viscosity terms are stabilizing for $m < 1$ and destabilizing for $m > 1$. For a large ratio of surface tension to viscous forces, and for $m < 1$, they also find a band of Reynolds numbers for which viscosity stratification can prevent capillarity from destabilizing the interface to leading order in the ratio, ε, of the undisturbed annulus thickness to core radius. To leading order in ε, a fluid–fluid density difference contributes a purely imaginary term to the growth of an interfacial disturbance, i.e. its contribution is purely dispersive.

Frenkel *et al.* (1987) considered a core–annular flow of fluids with matched viscosities and densities in the thin annulus limit, where lubrication theory governs the annulus flow. (Section 3 discusses lubrication theory, the balancing of the axial derivative of the pressure with the term involving the curvature of the axial velocity in the axial component of the Navier–Stokes equation to leading order in ε, in more detail.) They also chose parameters where the flow in this simplified annulus fully determines the interface stability to leading order in ε. The base flow contribution to the convective term in the kinematic condition, evaluated at the disturbed interface position, yielded the (weakly) nonlinear term in the resulting Kuramoto–Sivashinky (KS) equation for the interface position. In the appropriate parameter regimes, this

equation's dynamics cause linearly unstable long waves to saturate in the weakly nonlinear regime. Papageorgiou, Maldarelli & Rumschitzki (1990) considered the effect of parameter scales that, for $m \neq 1$, resulted in the (non-lubrication) core dynamics contributing non-local terms to the leading-order equation for the interface motion to systematically develop more general amplitude equations that govern the interface dynamics. These equations resemble Kuramoto–Sivashinky equations, but include, in addition to the nonlinear and capillary-derived terms, these non-local viscosity stratification terms. These studies indicate that the nonlinear term deriving from the base flow steepens interfacial deflections in the nonlinear regime. Such steepening gives rise to shorter length-scale axial interface waves, whose amplitude is strongly suppressed by capillary forces. This combination of effects saturates the growth of linearly unstable long waves, and can lead to either chaotic interfacial motions or nonlinear travelling waves. Kerchman (1995) requires negligible interface shear, but allows interface disturbances of sizes comparable to the film thickness to examine strongly nonlinear CAF interface dynamics. He finds that, for surface tensions much larger than those leading to Papageorgiou *et al.*'s equations, the CAF arrangement may collapse. In the absence of a base flow, linearly unstable disturbances also grow through the weakly nonlinear regime, which suggests that either the core will snap off or the annular layer will rupture (Hammond 1983). As such, the stability of a CAF with a clean interface is fairly well understood.

Studies of the effects of surfactants on the stability of CAFs are motivated by applications in oil recovery (Babadagli 2003), pulmonary diseases due to airway closure (Otis *et al.* 1993), as well as surfactant replacement therapy (SRT) using liquid boluses (Espinosa & Kamm 1999). In liquid–liquid displacements common in oil recovery, the displacing fluid can finger into the oil. A high interfacial tension can cause the wetting layer to snap and bring the non-wetting phase in contact with the capillary pore wall. Contact line forces attaching the slug to the wall can retard train mobility, thereby making recovery more difficult. Experience shows that adding surfactant reduces the surface tension, and thus improves the recovery efficiency. In the lung, air travels through a hierarchy of bronchioles whose inner surfaces are coated by a thin layer of mucus. This cylindrical liquid layer typically maintains its integrity during respiration owing to the surfactant 1,2-dipalmitoyl phosphatidylcholine (DPPC) produced in the lung. DPPC retards the time needed for the growth of the capillary instability to times long compared with a breathing cycle. In premature infants and adults with adult respiration distress syndrome (ARDS), this surfactant may be insufficient or may not function properly. As a result, capillary forces can amplify interface disturbances to the point of blocking airways and inhibiting respiration. Clearly, to prevent airway closure, one would like to discourage the capillary instability. Surfactant replacement therapy (SRT) is often used as the remedy for such surfactant deficiency. One method of SRT instills liquid as a vehicle to deliver exogenous surfactants into the lung. Such liquid often forms a liquid plug that leaves trailing films behind and/or ahead of it. Rather than having to deal with airway closure, one must, with SRT, appropriately manage, e.g. via breathing rates, the formation of liquid plugs to deliver sufficient surfactant from one airway generation to another.

Otis *et al.* (1993) developed a lubrication model to examine airway closure in the presence of insoluble surfactants, but in the absence of a base flow. They showed that surfactants slow the process of airway closure because flows generated by Marangoni stresses act against those generated by capillarity. Cassidy *et al.* (1999) later carried out experiments and compared their results with a flexible-tube model (Halpern & Grotberg 1993) in the limit of a rigid tube. They found that surfactants decrease the linear growth rate to 1/4 that of the clean interface when the interface becomes

tangentially immobile. It is worth pointing out that Carroll & Lucassen (1974) found the same reduction of the growth rate when they examined the effects of surfactants on the linear stability of a fluid layer coating the exterior surface of a cylinder. In the Stokes flow regime, the linear stability of a jet with surfactants similarly showed a slower growth rate than that of a clean jet (Craster, Matar & Papageorgiou 2002), and that the wavelength of maximum instability increased with increasing surfactant activity (as codified by the elasticity number introduced below); the trends were more subtle elsewhere (Hansen, Peters & Meijer 1999). Kwak & Pozrikidis (2001) found the presence of an insoluble surfactant at the interface of two concentric fluid layers in an annulus to be stabilizing. All of these studies considered the liquid layer to be Newtonian and, in § 6, we address the applicability of such models to the lung.

None of these studies of how the presence of surfactants impacts the stability of a cylindrical fluid–fluid interface considers a base flow. Only a few related investigations include base flows, and generally only in rectangular geometry. Whitaker & Jones (1966) and Lin (1970) performed a long-wave analysis of the stability of a falling film in the presence of surfactants. They showed that insoluble surfactants could stabilize a falling film and increase the marginal Reynolds number for instability. Pozrikidis (2003) numerically solved for the eigenvalues for arbitrary wavelength eigenfunction disturbances in the Stokes flow limit. He found that, although the system with surfactant remains stable, it has less negative growth rates than the surfactant-free system. Ji & Setterwall (1994) numerically studied the impact of soluble surfactants on the linear stability of a vertical falling film. In addition to surfactant-induced stabilization, i.e. damping, of surface waves, an instability for short and moderate waves associated with Marangoni forces arises at low Reynolds numbers. For long waves, Marangoni forces destabilize in a manner analogous to the situation in the thermocapillary instability of a falling liquid layer down a heated plane (Smith 1990; Goussis & Kelly 1991). Dijkstra & Steen (1991) studied the linear stability of a thermocapillary-driven flow on the exterior surface of the cylinder. They showed that complete stabilization may occur under some circumstances.

Frenkel & Halpern (2002) and Halpern & Frenkel (2003) (hereinafter referred to as FH and HF, respectively) studied the stability of a two-dimensional planar two-layer Couette–Poiseuille flow between parallel plates in the presence of an insoluble surfactant. Their analysis showed that, with flow, the surfactant could destabilize the interface (if the base state has a non-zero interfacial shear), even though it is stable without surfactant. (FH refer to an earlier draft of this work (minus the Appendix) which, as below, centres on the emergence of this flow-induced Marangoni-driven instability on a cylindrical interface in a core–annular flow.) Blyth & Pozrikidis (2004) later demonstrated that such a Marangoni instability can be arrested by nonlinear effects. This line of work shows that a base shear flow can induce surfactant gradients, and the work in the last paragraph shows that interfacial growth can induce surfactant gradient-generated Marangoni forces that interact with capillary forces. By studying a core–annular flow in the presence of surfactants, the present work combines these effects to see how flow-derived surfactant-gradient-generated Marangoni forces compete with capillary forces in a single system. (The size of the capillary number modulates, here in the presence of Marangoni forces, between the limiting cases of capillary forces being dominant and being negligible relative to viscous forces.) It is this competition that is, in fact, critical in applications such as oil recovery and in the liquid lining of small lung airways, and can lead to situations that are more or less stable than analogous clean interface systems. FH and HF consider a planar geometry

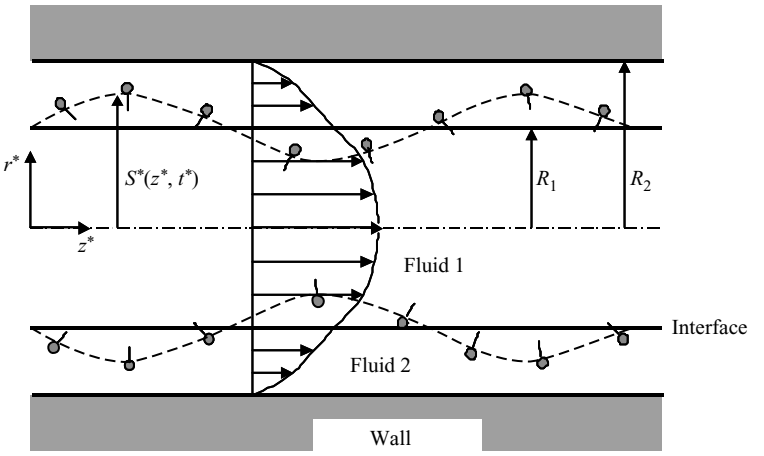

FIGURE 1. The geometry of a core–annular flow in the presence of insoluble surfactants. $r^* = S^*(z^*, t^*)$ is the equation for the fluid–fluid interface.

and thus do not have this competition. Since most such applications of CAFs have thin annular layers, we examine this problem analytically in the asymptotically thin annulus limit (Papageorgiou *et al.* 1990; Georgiou *et al.* 1992), a limit that is difficult to resolve computationally. FH and HF are restricted to Stokes flow. Our treatment below has much weaker Reynolds number Re constraints, allowing, e.g. core $Re_1 = O(1)$, thereby including a broader range of flows. The thin-annulus limit does this because, in appropriate parameter regimes, it yields leading-order equations containing only annulus variables. Thus, the non-trivial effects of viscous stratification (Yih 1967; Preziosi *et al.* 1989; Papageorgiou *et al.* 1990) are (analytically) absent from the problem, despite non-zero Re.

Section 2 defines the complete set of governing equations and the base-state solution. Section 3 carefully analyses the scales of each of the dynamic variables in terms of those of the parameters and derives consistent sets of scales that lead to non-trivial evolutions. The major assumption here is a separation of length scales in the fluid annulus, with its radial scale being much shorter than its axial scale. Capillary-number restrictions ensure that the leading-order interface dynamics are determined solely by the annulus equations, without a contribution from the core. The Appendix considers the alternative scenario of no scale separation, but of zero Reynolds number, i.e. Stokes flow, and provides the opportunity for independent checks of both formulations in their mutual limit. Section 4 formulates and solves the linear stability problem with the scales from § 3. Section 5 analyses the stability results in a number of limiting parameter regimes and, from such analyses, develops physical insight into the mechanisms at work. It makes comparison with FH/HF whenever similar issues are addressed. Finally, § 6 gives numerical examples related to the motivating applications, and § 7 summarizes.

2. Base state, governing equations and boundary conditions

Two immiscible viscous incompressible fluids are flowing axisymmetrically in a core–annular arrangement in a straight tube with radius R_2 (see figure 1). Let $*$ denote a dimensional variable. The interface is given by $r^* = S^*(z^*, t^*)$, with r^*, z^*, t^* being the radial and axial cylindrical coordinates and time, respectively. Fluid 1, with viscosity

μ_1, occupies the core region $0 \leqslant r^* \leqslant S^*(z,t)$; fluid 2, having viscosity μ_2, fills the annular region $S^*(z^*,t^*) \leqslant r^* \leqslant R_2$. The densities of both fluids are matched and denoted by ρ. Because the flow fields and the perturbations (after Hickox 1971) are assumed to be axisymmetric (no θ-dependence), we only consider velocity components $\boldsymbol{v}^* = (u^*, 0, w^*)$ in terms of the cylindrical coordinates (r^*, θ, z^*). To study the linear stability of the system, we begin with the unperturbed or base state. Let $r^* = R_1$ be the unperturbed, cylindrical interface. Define the jump notation $[\cdot] := (\cdot)_1 - (\cdot)_2$. For a flow driven by a uniform pressure gradient $\nabla^* p^* = -F\boldsymbol{e}_{z^*}$ with $F > 0$, the base state is

$$\boldsymbol{v}^* = (0, 0, \overline{w}^*(r^*)),\ [\overline{p}^*] = \frac{\sigma_0^*}{R_1},\ \overline{\Gamma}^* = \Gamma_0^*, \tag{2.1}$$

where

$$\overline{w}^*(r^*) = -\frac{F}{4\mu_1}\left(r^{*2} - R_1^2\right) + \frac{F}{4\mu_2}\left(R_2^2 - R_1^2\right) \quad \text{for } 0 \leqslant r^* \leqslant R_1, \tag{2.2a}$$

$$\overline{w}^*(r^*) = \frac{F}{4\mu_2}\left(R_2^2 - r^{*2}\right) \quad \text{for } R_1 \leqslant r^* \leqslant R_2. \tag{2.2b}$$

The unperturbed, insoluble surfactant concentration, Γ_0^*, is uniform along the unperturbed interface and the corresponding interfacial tension is σ_0^*. Because we perform only a linear stability analysis, without loss of generality, we expand the equation of state $\sigma^*(\Gamma_0^*)$ in a Taylor series:

$$\sigma^* = \sigma_0^* - \beta(\Gamma^* - \Gamma_0^*) - \gamma(\Gamma^* - \Gamma_0^*)^2 + O((\Gamma^* - \Gamma_0^*)^3), \tag{2.3}$$

where $\beta = -(\partial\sigma^*/\partial\Gamma^*)_{\Gamma_0^*}$ and $\gamma = -(1/2)(\partial^2\sigma^*/\partial\Gamma^{*2})_{\Gamma_0^*}$ and truncate after the linear term.

To non-dimensionalize, we choose R_1 as the characteristic length, and scale velocities with the centreline velocity $W_0 = F(R_1^2(\mu_2 - \mu_1) + R_2^2\mu_1)/(4\mu_1\mu_2)$. The pressure is scaled inertially with ρW_0^2 and time with R_1/W_0. The surfactant concentration is scaled with Γ_0^* and the interfacial tension with σ_0^*. Define the viscosity ratio $m = \mu_2/\mu_1$ and the radius ratio $a = R_2/R_1$. The non-dimensional base state becomes

$$\left.\begin{aligned} \overline{w}(r) &= 1 - \frac{mr^2}{(a^2 + m - 1)} \quad \text{for} \quad 0 \leqslant r \leqslant 1, \\ \overline{w}(r) &= \frac{(a^2 - r^2)}{(a^2 + m - 1)} \quad \text{for} \quad 1 \leqslant r \leqslant a, \\ [\overline{p}] &= \frac{1}{Re_1 Ca},\ \overline{\Gamma} = 1, \end{aligned}\right\} \tag{2.4}$$

where $Re = Re_1 = \rho W_0 R_1/\mu_1$ is the Reynolds number, $Ca = \mu_1 W_0/\sigma_0^*$ is the capillary number, and both are based on core (fluid 1) quantities. The non-dimensional equation of state becomes

$$\sigma = 1 - El(\Gamma - 1), \tag{2.5}$$

where $El = \beta\Gamma_0^*/\sigma_0^*$ is the elasticity number and, again, we retain only the linear term from (2.3).

Let subscripts r, z and t denote partial differentiation, $\nabla^2 = \partial^2/\partial r^2 + (1/r)(\partial/\partial r) + \partial^2/\partial z^2$ and the fluid 2 Reynolds number $Re_2 = Re_1/m$. The non-dimensional governing

equations for each fluid are

$$\frac{1}{r}(ru)_r + w_z = 0, \tag{2.6a}$$

$$w_t + uw_r + ww_z = -p_z + \frac{1}{Re_i}\nabla^2 w, \tag{2.6b}$$

$$u_t + uu_r + wu_z = -p_r + \frac{1}{Re_i}\left(\nabla^2 u - \frac{1}{r^2}u\right), \tag{2.6c}$$

Hereinafter the subscripts 1 and 2 denote the fluid regions. The system is subject to the following boundary conditions: the velocities vanish at the wall; u_1 and $\partial w_1/\partial r$ are zero at $r = 0$.

$$w_2 = u_2 = 0 \text{ at } r = a; \qquad u_1 = w_{1r} = 0 \text{ at } r = 0. \tag{2.7}$$

Velocities are continuous at the interface,

$$[w] = 0, [u] = 0 \text{ on } r = S(z,t). \tag{2.8a, b}$$

The tangential stress and normal stress balances at the interface $r = S(z,t)$ are

$$\frac{1}{\left(1+S_z^2\right)^{1/2}}\left[\frac{1}{Re}(u_z + w_r)\left(1 - S_z^2\right) + \frac{2}{Re}(u_r + w_z)S_z\right] = \frac{-El}{CaRe_1}\Gamma_z, \tag{2.9}$$

$$-\left[p - \frac{2}{Re}u_r - \left(-p + \frac{2}{Re}w_z\right)S_z^2 + \frac{2}{Re}(u_z + w_r)S_z\right] = \frac{\sigma(\Gamma)}{CaRe_1}\left(S_{zz} - \frac{1}{S}\left(1 + S_z^2\right)\right)\left(1 + S_z^2\right)^{-3/2}, \tag{2.10}$$

where (2.5) gives $\sigma(\Gamma)$. The kinematic condition, in either core or film variables, is

$$u = S_t + wS_z \text{ on } r = S(z,t). \tag{2.11}$$

Finally, we assume that surfactant diffusion is negligible here. Thus the surfactant transport equation for insoluble surfactants along the interface is (Waxman 1984; Wong, Rumschitzki & Maldarelli 1996):

$$\Gamma_t - \frac{S_t S_z}{1+S_z^2}\Gamma_z + \frac{1}{S\sqrt{1+S_z^2}}\left(\frac{S(w+uS_z)}{\sqrt{1+S_z^2}}\Gamma\right)_z + \frac{(u - wS_z)}{\left(1+S_z^2\right)^2}\left(\frac{1+S_z^2}{S} - S_{zz}\right)\Gamma = 0. \tag{2.12}$$

To combine the first two terms of (2.12) into a single partial derivative with respect to time, corresponds to prescribing that coordinate points on the surface advance in time in the direction normal to the interface or, as Waxman puts it, 'fixed coordinates'. The third term represents surface convection and the fourth term reflects the effect of dilation or contraction of the interface.

3. Scaling analysis

With the base state as the above, we now begin the corresponding linear stability analysis. Let ε be the ratio of the undisturbed annulus thickness to core radius. In this section we begin by performing a scaling analysis, and then derive the linear stability equations from the leading-order equations and boundary conditions. These results are based on lubrication in the annulus, which requires that the length scale

over which the dynamic variables change in the radial direction be much smaller than the scale over which they change in the axial direction in the annulus, i.e. $\varepsilon \ll 1$. We consider only perturbations whose wavelengths are long compared with the annulus thickness. If, in addition, $m/(\varepsilon^2 Re_1) \gg \varepsilon$ and much greater than the inverse of the non-dimensional time scale over which velocities change (note the base axial velocity $\overline{w}$ in the annulus is of order ε), then the terms mw_{rr}/Re_1 and the axial pressure gradient dominate (2.6*b*). Thus, lubrication in the annulus is valid for non-zero Reynolds numbers as long as $Re_1 \ll m/\varepsilon^3$. (We discuss conditions under which the annulus alone dictates the leading-order interface equation below.) Alternatively, the Appendix derives the stability equations for zero Re and no *a priori* scale separation. We can scale these equations and extract their leading order or solve them numerically.

The thin-film limit ($\varepsilon \ll 1$) allows us to introduce a stretched film variable $y := 1 - (r-1)/\varepsilon$, which explicitly expresses that radial derivatives $\partial/\partial r = -(1/\varepsilon)(\partial/\partial y)$ are large. For a viscosity ratio $m = O(1)$, the leading order (in ε) base flows in the film and core, respectively, are

$$\overline{w} = \frac{2\varepsilon}{m} y + O(\varepsilon^2), \quad \overline{W} = (1 - r^2) + O(\varepsilon). \tag{3.1a, b}$$

We allow an infinitesimal (of order $\delta_1 \ll \varepsilon$), axisymmetric perturbation to the steady circular interface and a corresponding disturbance of size $\delta_2 \ll \varepsilon$ to the uniform surfactant concentration:

$$S(z, t) = 1 + \delta_1 \eta(z, t), \tag{3.2}$$

$$\Gamma(z, t) = 1 + \delta_2 G(z, t). \tag{3.3}$$

To estimate the scales of the perturbed quantities, we follow a scaling procedure similar to those used in Hammond (1983), Papageorgiou *et al.* (1990) and Georgiou *et al.* (1992). Let (w'', u'', p'') and (W'', U'', P'') represent the perturbed quantities for the film and the core, respectively, e.g. $w = \overline{w} + w''$, etc. In the thin-film lubrication limit, a perturbation, $\delta_1 \eta(z, t)$, to the interface causes a large (typically scaling as $\varepsilon^{-2} w''/Re_1$ with ε, cf. (2.6*b*) and below) perturbation pressure $p'' \sim \delta_1/(Re_1 Ca)$ in the thin annulus that drives the perturbation flow in the film. These dynamics couple to the interface and dictate its stability. In the present situation, however, surface tension gradients deriving from perturbations to the surfactant distribution can also induce interfacial flows and, by continuity, flows in the core and film. We begin by considering the perturbation flows driven by the capillary pressure from the perturbed interface; we call this the strong tension, i.e. low Ca, case and derive the corresponding scalings. We then consider the weaker tension, i.e. higher Ca, case, where the dominant mechanism that drives the flow shifts from the capillary pressure to the Marangoni flow induced by the surfactant concentration gradient.

As just noted, capillarity, for an interfacial deflection, $\delta_1 \eta$, induces a perturbed pressure, $p'' \sim \delta_1/Re_1 Ca$, via the normal stress balance (2.10). A perturbation, $\delta_2 G(z, t)$, to the uniform surfactant distribution – surfactant contamination – also induces a surface tension gradient via $\sigma(\Gamma) = 1 - \delta_2 El G$ and produces a perturbation pressure, $p'' \sim \delta_2 El/(Re_1 Ca)$, through the normal stress balance. As we shall see below, for the low Ca scalings, both scalings for the induced pressure perturbation are proper and consistent, but the former scaling is of lower order in ε.

We begin with the capillary scaling for the perturbed pressure and check the consistency of this scaling *a posteriori*. The equations of motion and continuity, (2.6*a*)–(2.6*c*), for the film, result in disturbed velocity scales: $w'' \sim \varepsilon^2 \delta_1/(mCa)$ and $u'' \sim \varepsilon^3 \delta_1/(mCa)$. If we introduce a long time scale, $\tau^* = \varepsilon t/m$ (assuming $m \gg \varepsilon$), and assume for linear

stability that δ_1 is infinitesimal relative to ε, then a balance of terms in the kinematic condition (2.11) leads to

$$Ca \sim \varepsilon^2, \tag{3.4}$$

which corresponds to the strong surface tension regime. It is well known (Frenkel *et al.* 1987), and easy to see (see below), that, in this regime ($Ca \ll \varepsilon$), the core dynamics are slaved to the annulus dynamics. The resulting perturbed film quantities are $w'' \sim \delta_1/m$, $u'' \sim \varepsilon\delta_1/m$ and $p'' \sim \delta_1/(\varepsilon^2 Re_1)$. For the core region, the continuity of the axial velocity across the interface and the lack of a separation of scales determine the scalings of the perturbed core quantities as $W'' \sim \delta_1/m$, $U'' \sim \delta_1/m$ and $P'' \sim \delta_1/(mRe_1)$. The tangential stress condition now balances the film's viscous stress and the Marangoni stress to give $\varepsilon\delta_1/Ca \sim \delta_2 El/Ca$, or

$$\delta_2 \sim \delta_1 \varepsilon/El. \tag{3.5}$$

Since $Ca \sim \varepsilon^2$, if the Marangoni number, $Ma := \beta\Gamma_0^*/(\mu_1 W_0) = El/Ca = O(1)$, which can occur in surfactant replacement therapy using exogenous surfactants for various airflow conditions in different airway generations (Halpern, Jensen & Grotberg 1998), the induced perturbation, δ_2, to the surfactant concentration is an order of ε lower (i.e. larger) than the interfacial perturbation, δ_1. Recall that surfactant contamination causes a perturbation in the film's pressure of order $\delta_2 El/(Re_1 Ca) \sim \delta_1\varepsilon/(Re_1 Ca)$ that, in this case, is of a higher order in ε than the capillary pressure perturbation, $\delta_1/(Re_1 Ca)$. Note also that, as the normal stress condition, the leading-order tangential stress condition (2.9) now involves only film quantities; thus, the film problem is closed without reference to the core. That is, the film solution governs the linear interfacial stability, and these are inputs to the core dynamics problem.

Finally, we check that (3.5) is consistent with the scaling results from the perturbed surfactant transport equation (2.12). The leading order of (2.12) is

$$(\varepsilon\delta_2/m)G_{\tau^*} + \overline{w}(1)\delta_2 G_z - \frac{1}{\varepsilon}\overline{w}_y|_{y=1}\delta_1\eta_z\overline{\Gamma} + w_z''\overline{\Gamma} = O(\varepsilon\delta_1), \tag{3.6}$$

where we have invoked the same long time scale, $\tau^* = \varepsilon t/m$, used in the kinematic condition, and where we have retained $\overline{\Gamma}(=1)$ here to facilitate interpretation of the terms. The lead term ($O(\varepsilon\delta_2/m)$) is the local time rate of change of surfactant concentration, and the other terms all derive from the $\nabla_s\cdot(\boldsymbol{v}_s\Gamma)$ (where $\boldsymbol{v}_s$ is the projection of the interface velocity into the interface's tangent plane), the third term of (2.12), in the surfactant balance. The second ($O(\varepsilon\delta_2/m)$) and fourth ($O(\delta_1/m)$) terms in (3.6) are the surface convective terms due to the base flow's interface ($\overline{w}(1) = 2\varepsilon/m$) and perturbation ($w'' \sim \varepsilon^2\delta_1/mCa \sim \delta_1/m$) velocities. The third term, $O(\delta_1/m)$, arises from the change in the base flow's axial velocity, $\overline{w} = 2\varepsilon y/m$, owing to its being evaluated at the displaced interface. The remaining terms in (2.12), due to the stretching of the interface (the fourth term of (2.12)) and the motion of the surface coordinates, are of order $O(\varepsilon\delta_1)$, $O(\varepsilon\delta_1/m)$ or higher. Therefore, the scaling (3.5) is consistent with retaining all of the convective terms in (3.6) when $El \sim \varepsilon^2$ or $Ma \sim 1$. If El is of a lower order, say $\sim\varepsilon$, then, from (3.5), $\delta_2 \sim \delta_1$. In this case, (3.6) becomes $-(1/\varepsilon)\overline{w}_y|_{y=1}\delta_1\eta_z\overline{\Gamma} + w_z''\overline{\Gamma} = O(\varepsilon\delta_2)$, in which the time-derivative, $(\varepsilon\delta_2/m)G_{\tau^*}$ and the convective term, $\overline{w}(1)\delta_2 G_z$, would enter at the next order. As we shall see in § 5.3, this occurs for the immobile interface owing to the relatively large *Ma*.

The above scalings are based on the supposition that the capillary pressure from the perturbed interface drives the film's flow, and this requires the strong surface tension of (3.4). We now consider another limiting case where the surface tension is weaker,

i.e. $Ca \gg \varepsilon^2$. In that case, the surface tension gradient due to the perturbed surfactant concentration can drive the perturbed flows via the tangential stress condition; this yields the estimate $w'' \sim \varepsilon\delta_2 Ma/m$, with $u'' \sim \varepsilon^2\delta_2 Ma/m$ from continuity. The normal stress condition yields $p'' \sim \delta_2 Ma/Re_1$. This is also the scaling of the pressure term in the axial component of the equation of motion, but it is dominated there by the viscous term, $(m/\varepsilon^2 Re_1)w'' \sim \delta_2 Ma/(\varepsilon Re_1)$. Thus, the perturbation flow does not derive from the perturbation pressure and we do not expect to see the capillary instability in this limit. The kinematic condition for the long time scale, $\tau^* = \varepsilon t/m$, gives $\delta_2 \sim \delta_1/(\varepsilon Ma)$; this yields $w'' \sim \delta_1/m$, $u'' \sim \varepsilon\delta_1/m$ and $p'' \sim \delta_1/(\varepsilon Re_1)$. The perturbed core quantities all retain the same orderings as in the previous case and its dynamics are again slaved to those of the film.

The leading-order surfactant transport equation, (3.6), again has first and second terms with scaling $\varepsilon\delta_2/m$ unchanged, while the third and fourth terms are of orders δ_1/m and $\varepsilon\delta_2 Ma/m$, respectively. For $Ma = O(1)$, all of the terms in (3.6) are comparable again. In § 5, we shall see, for $Ma = O(1)$, that this is a formal zero surface-tension limit of the previous case.

4. Formulation of the leading-order linear stability

With the scalings (3.4) and (3.5), we now formulate the linear stability problem, and make the scalings of the disturbance quantities explicit, e.g. $w'' = (\delta_1/m)w'$. Typically for applications in liquid–liquid displacements, $Re_1 = O(1)$ or less and Re in the thin film is an order of ε higher. Section 3 postulates the perturbed film (small) and core (capital) quantities as

$$w = \overline{w} + \frac{\delta_1}{m}w' + O\left(\frac{\varepsilon\delta_1}{m}\right), \quad u = \frac{\varepsilon\delta_1}{m}u' + O\left(\frac{\varepsilon^2\delta_1}{m}\right), \quad p = \overline{p} + \left(\frac{\delta_1}{\varepsilon^2}\right)p' + O\left(\frac{\delta_1}{\varepsilon}\right), \tag{4.1a}$$

$$W = \overline{W} + \frac{\delta_1}{m}W' + O\left(\frac{\varepsilon\delta_1}{m}\right), \quad U = \frac{\delta_1}{m}U' + O\left(\frac{\varepsilon\delta_1}{m}\right), \quad P = \overline{P} + \frac{\delta_1}{m}P' + O\left(\frac{\varepsilon\delta_1}{m}\right). \tag{4.1b}$$

After substitution of (4.1) into (2.6), the governing equations for the film become

$$u'_y = w'_z, \tag{4.2a}$$

$$0 = -p'_z + \frac{1}{Re_1}w'_{yy}, \tag{4.2b}$$

$$0 = -p'_y. \tag{4.2c}$$

Thus, the perturbed film pressure p' remains uniform across the film and the solutions

$$w' = \tfrac{1}{2}Re_1 p'_z y^2 + Ay, \tag{4.3a}$$

$$u' = \tfrac{1}{6}Re_1 p'_{zz} y^3 + \tfrac{1}{2}A_z y^2, \tag{4.3b}$$

satisfy no slip at the wall, $y = 0$. Using (4.1), expanding the base state interfacial velocities about their values at the base state interface, $r = S = 1$, and invoking the facts $Ca = Ca_0\varepsilon^2$ and $\delta_1 = \varepsilon\delta_2$, we find that the tangential and normal stress balances, (2.9) and (2.10), become

$$w'_y = -MaG_z, \tag{4.4}$$

$$p' = \frac{1}{Re_1 Ca_0}(\eta + \eta_{zz}), \tag{4.5}$$

where $Ca_0 = Ca/\varepsilon^2 = O(1)$. Equation (4.4) allows solution for A in (4.3), which leads to:

$$w' = Re_1 p'_z\left[\tfrac{1}{2}y^2 - y\right] - MaG_z y, \tag{4.6a}$$

$$u' = Re_1 p'_{zz}\left[\tfrac{1}{6}y^3 - \tfrac{1}{2}y^2\right] - \tfrac{1}{2}MaG_{zz}y^2, \tag{4.6b}$$

where (4.5) gives p'. The leading-order ($O(\varepsilon\delta_1/m)$) kinematic condition, (2.11), is

$$u'(y=1) = \eta_{\tau^*} + 2\eta_z. \tag{4.7}$$

If $Ma = O(1)$, then the surfactant transport equation, (2.1), has the same form as (3.6):

$$G_{\tau^*} + 2G_z - 2\eta_z + (w'(y=1))_z = 0, \tag{4.8}$$

where we have again introduced a long time scale, $\tau^* = \varepsilon t/m$, in (4.7)–(4.8) in order to arrive at non-trivial evolutions. Substitution of (4.6) with (4.5) into (4.7) and (4.8) yields the following coupled set of equations governing the leading-order linear stability of the system:

$$\eta_{\tau *} + 2\eta_z + \frac{1}{3Ca_0}(\eta_{zz} + \eta_{zzzz}) + \tfrac{1}{2}MaG_{zz} = 0, \tag{4.9a}$$

$$G_{\tau *} + 2G_z - 2\eta_z - \frac{1}{2Ca_0}(\eta_{zz} + \eta_{zzzz}) - MaG_{zz} = 0. \tag{4.9b}$$

Note that m is absent from (4.9); since the core is decoupled from the problem, the viscosity ratio m should be irrelevant. (μ_1 appears because we chose to define Ca_0 and Ma with μ_1 rather than μ_2 since we scaled velocities with W_0.) As such, the time scale, $\tau^* = \varepsilon t/m$, suggests that the growth rate scales as $1/\mu_2$, i.e. the more viscous the film, the slower the fluid motions. Another consequence is that the marginal wavelength does not depend on m. Also notice that even though the perturbed pressure and velocities depend on the Reynolds number (owing to the scalings), (4.9) depends on Ca rather than Re. This is also natural, since the leading-order film equations are inertia-free and the perturbation flows are surface-tension driven.

The leading-order governing equations for the core flow are

$$\frac{1}{r}(rU')_r + W'_z = 0, \tag{4.10a}$$

$$-2rU' + (1-r^2)W'_z = -P'_z + \frac{1}{Re_1}\nabla^2 W', \tag{4.10b}$$

$$(1-r^2)U'_z = -P'_r + \frac{1}{Re_1}\left(\nabla^2 U' - \frac{U'}{r^2}\right), \tag{4.10c}$$

subject to the following leading-order boundary conditions:

$$W'(r=1) = (2-2/m)\eta + w'(y=1), \quad U'(r=1) = 0. \tag{4.11}$$

The dynamics of the core can be expressed in terms of Kummer's confluent hypergeometric functions, as in Papageorgiou *et al.* (1990). The only differences between our core equations and theirs are the inclusion of m in the time scaling (see the last paragraph) and the presence of the term $w'(y=1)$ (owing to the different scalings here), already determined from the solution to (4.9), in the boundary condition containing $W'(r=1)$. Since the core flow first influences the stability problem one order higher in ε than the leading order, we do not carry out its calculation here.

Notice that, as in Georgiou *et al.* (1992), our theory is based on lubrication in the film, which requires that the radial length scale in the annulus be much shorter than the axial scale. Thus, its predictions only hold for perturbation wavelengths, scaled by the core radius, that are large compared with ε. The film's lubrication breaks down when the perturbation wavelength is comparable to the film thickness; so this theory says nothing about very short wavelength disturbances, i.e. large longitudinal curvature, that capillary forces are known to act to stabilize.

5. The system's leading-order linear stability: results and analysis

5.1. *No base flow case* (*strong tension limit*)

Hereinafter, in discussing stability, we find it convenient (and consistent with previous studies: Georgiou *et al.* 1992; Wei & Rumschitzki 2002, etc.) to use the time scale $\tau = \varepsilon t$, rather than τ^*, which transfers the m-dependence from the time scale back into the equations. This introduces $1/m$ into all of the terms in (4.9) other than those with time derivatives.

As a reference or control case, we begin by examining how Marangoni forces deriving from the presence of insoluble surfactants compete with capillary forces in the absence of a base flow. As noted, Otis *et al.* (1993) and others already considered this case in various limits. This subsection just recovers established results in the zero flow limit. Without a base flow, the velocity and the time scales cannot rely on the centreline velocity; instead we choose the capillary scales σ_0^*/μ_1 and $R_1\mu_1/\sigma_0^*$, respectively. The corresponding pressure scale is σ_0^*/R_1 and the resulting Reynolds number is $Re_1 = \rho(\sigma_0^*/\mu_1)R_1/\mu_1$, called J by Preziosi *et al.* (1989) and others (e.g. Papageorgiou *et al.* 1990; Georgiou *et al.* 1992), which is the inverse of the Ohnesorge number. Since, with the capillary velocity, there is no longer a meaningful capillary number, the ratio of Marangoni to surface tension forces is reflected by *El*. A scaling procedure similar to that in § 3 yields $El \sim \varepsilon^2$ and (3.5). Let $El = \varepsilon^2 El_0$. A procedure similar to that in § 4 yields

$$\eta_T + \frac{1}{3m}(\eta_{zz} + \eta_{zzzz}) + \frac{El_0}{2m}G_{zz} = 0, \tag{5.1a}$$

$$G_T - \frac{1}{2m}(\eta_{zz} + \eta_{zzzz}) - \frac{El_0}{m}G_{zz} = 0, \tag{5.1b}$$

where we have introduced a long time scale, $T = \varepsilon^3 t$ (now in units of $R_1\mu_1/\sigma_0$). Notice that since the system only has the capillary velocity scale in this limit, neither *Ca* nor *Ma* appears in (5.1). Comparison shows (5.1) to be consistent with (4.9) in the small *Ca*, i.e. in the very strong tension limit: Simply replace $Ma = El_0/Ca_0$, rescale time as $T = Ca_0^{-1}\tau$, and take the (formal) limit $Ca_0 \to 0$. This corresponds to taking $Ca \ll \varepsilon^2$, say ε^3. Clearly, very strong tension diminishes the importance of the base flow and the capillary instability dominates.

We takes normal modes $(\eta, G) = (\hat{\eta}, \hat{G})\exp(\mathrm{i}kz + sT)$ for (5.1), where k is the $O(1)$ disturbance wavenumber and s is an eigenvalue that is generally a complex number. Simple algebra leads to the solution for s, from the equations for $\hat{\eta}$ and $\hat{G}$, as:

$$\begin{gathered} s = \tfrac{1}{2}[-b(k) \pm \sqrt{b(k)^2 - 4c(k)}], \\ b(k) = \frac{El_0}{m}k^2 - \frac{1}{3m}k^2(1-k^2), \quad c(k) = -\frac{El_0}{2m}k^2\left[\frac{1}{6m}k^2(1-k^2)\right]. \end{gathered} \tag{5.2}$$

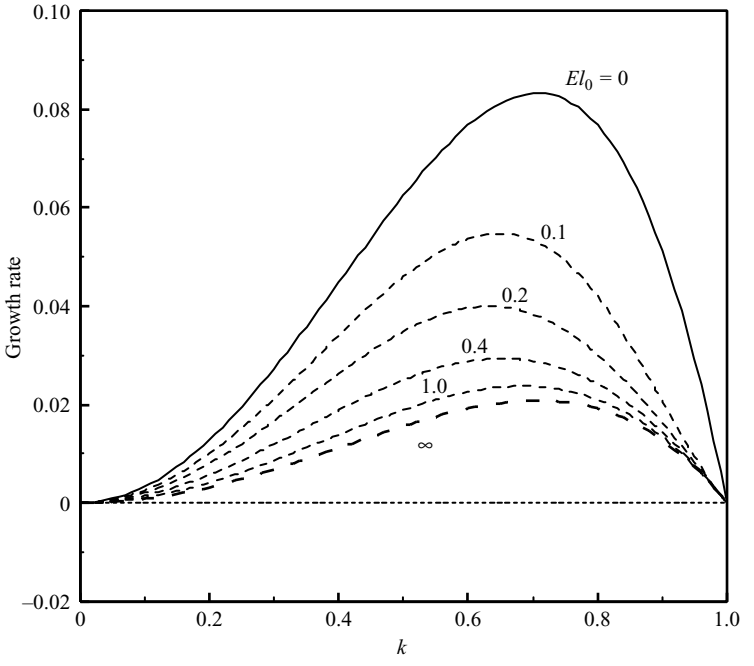

FIGURE 2. The zero base flow case: growth rates *vs.* k for the '+' mode in (5.2) for different El_0 and for $m = 1$.

It is easy to show that the discriminant in (5.2) is always non-negative. For a given k, figure 2 (as in Cassidy *et al.* 1999) shows the growth rate, s, corresponding to the + in (5.2) (this is the larger more dangerous mode) and its maximum, the most linearly unstable disturbance, for different El_0. $El_0 = 0$ in (5.2) recovers the classic clean interface capillary result:

$$s = \frac{1}{3m}k^2(1 - k^2), \tag{5.3}$$

which also follows from linearizing Hammond's equation (Hammond 1983). Long (short) waves $k < 1 (> 1)$ grow (decay) and the marginal wavenumber, $k_c = 1$. The growth rate decreases with increasing El_0 without change in k_c. This reduction of the growth rate is not simply the result of the surface tension reduction due to the presence of tension-lowering surfactant – this effect is negligible, since the tension $\sigma = 1 - El_0\varepsilon^2(\Gamma - 1)$ remains $1 + O(\varepsilon^2)$ – but rather to Marangoni retardation. The fact that k_c does not change suggests that the insoluble surfactant does not change the basic features of the capillary instability. For completeness, figure 3 illustrates the mechanism, similar to Otis *et al.* (1993), by which the surfactants affect the stability. Consider a long-wave ($k < 1$) interfacial disturbance. The circumferential curvature effect of capillarity causes the interfacial perturbation of the plus mode of (5.2) to grow by creating a gradient in the perturbed pressure that pushes fluid in the annulus from the crest towards the trough. This flow shears the interface, causing a tangential interfacial velocity that advects surfactants from the crest to the trough. This, in turn, induces a higher σ/ lower Γ at the crest and a lower σ/ higher Γ at the trough, which generates a Marangoni flow from the trough to the crest that opposes/slows the capillary growth. There are no changes for the surfactant concentration at node points since they experience no interfacial displacement during this process. The wavelength

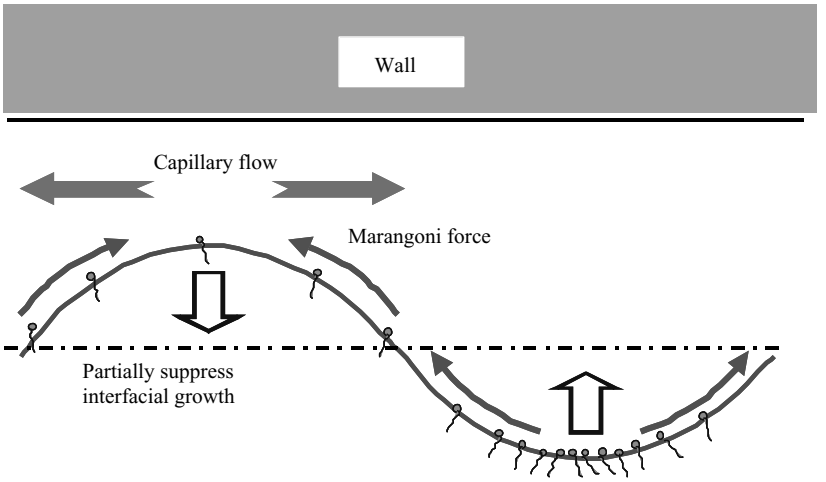

FIGURE 3. Illustration of the mechanism of how insoluble surfactants suppress long-wave capillary growth in the absence of a base flow. A perturbation to the interface drains fluid from the interface crest and pushes it towards the trough, thereby sweeping surfactant with it. The resulting surfactant gradient generates Marangoni forces that pull the interface back toward the crest, thereby slowing down/opposing the capillary-induced motion.

therefore does not change. This explains why the marginal wavenumber k_c does not change. Alternatively, the Marangoni force is purely a reaction to capillary growth, and thus does not change k_c.

In the eigenfunction for the minus mode for $k<1$, the amplitude ratio $\hat{G}/\hat{\eta}$ is again real and negative, but larger in magnitude than for the + mode, indicating that perturbations to the interfacial position and to the surfactant concentration are again out of phase. The surfactant perturbation is now larger, so that the interfacial Marangoni flows from the surfactant maxima to its minima are strong enough to overcome the capillary growth of long waves.

The growth rate reaches a non-zero minimum as $El_0\to\infty$. In this limit, the surfactant concentration becomes uniform and the interface becomes tangentially immobile; however, the interface still moves normally due to the capillary instability. Clearly, a tangential flow in the annulus will be slower for a tangentially immobile interface than for a stress-free one. As we examine (5.2) in the formal limit $El_0\to\infty (El\gg\varepsilon^2)$, we find

$$s=\frac{1}{12m}k^2(1-k^2). \tag{5.4}$$

As in Carroll & Lucassen (1974) and Cassidy *et al.* (1999), this is just 1/4 of s for the clean interface, (5.3). Alternatively, (5.4) is the interfacial evolution equation derived by replacing the tangential stress balance (4.4) with a tangentially rigid-interface condition $w'(y=1)=0$. We also find (5.4) via a large El_0 limit. For $\eta\sim O(1)$, (5.1*a*) suggests $G\sim 1/El_0$ (G almost uniform) as $El_0\to\infty$. Rescaling $G=\tilde{G}/El_0$ with $\tilde{G}=O(1)$ in (5.1) leads, at leading order in $1/El_0$, to

$$\eta_T+\frac{1}{3m}(\eta_{zz}+\eta_{zzzz})+\frac{1}{2m}\tilde{G}_{zz}=0, \tag{5.5a}$$

$$-\frac{1}{2m}(\eta_{zz}+\eta_{zzzz})-\frac{1}{m}\tilde{G}_{zz}+O\left(El_0^{-1}\right)=0. \tag{5.5b}$$

Eliminating $\tilde{G}_{zz}$ results in (5.5*c*), which also agrees with (5.4).

$$\eta_T + \frac{1}{12m}(\eta_{zz} + \eta_{zzzz}) = 0. \tag{5.5c}$$

As (5.5*c*) shows, an interfacial perturbation to a cylindrical interface with surface tension yields a pressure perturbation that contributes a destabilizing term η_{zz} attributable to the interface's circumferential curvature and a stabilizing term η_{zzzz} from its longitudinal curvature. In contrast, planar interfaces do not contain destabilizing surface tension-derived terms, and interfacial perturbations just recoil. Reasoning similar to figure 3 suggests that, without a base flow, insoluble surfactants make this recoil more sluggish.

5.2. *Weak tension limit*

The strong tension limit above corresponds to zero base flow. When the capillary pressure is absent, a perturbed surfactant distribution can generate a Marangoni force to drive a disturbed flow, yielding the equations

$$\eta_\tau + \frac{2}{m}\eta_z + \frac{Ma}{2m}G_{zz} = 0, \tag{5.6a}$$

$$G_\tau + \frac{2}{m}G_z - \frac{2}{m}\eta_z - \frac{Ma}{m}G_{zz} = 0. \tag{5.6b}$$

This is equivalent to the formal weak tension, $Ca_0 \to \infty$ limit ($Ca \gg \varepsilon^2$, e.g. $Ca = O(\varepsilon)$) of (4.9). As a result, capillary forces play no role, and (5.6) reflects how the base flow influences the effect of the Marangoni forces. The normal mode analysis for (5.6) gives

$$s = -\frac{2}{m}\mathrm{i}k + \frac{1}{2}\left[-\frac{Ma}{m}k^2 \pm \frac{Ma}{m}\sqrt{\frac{4\mathrm{i}}{Ma}k^3 + k^4}\right]. \tag{5.7}$$

Figure 4(*a*) shows the growth rates for different Ma *vs.* k (again, for the more dangerous + sign, the root with non-negative real part, in (5.7)) and figure 4(*b*) shows its $k \to 0$ limit. It also compares the $Ma = 1$ curve with the growth rate derived from the Stokes flow calculation in the Appendix for $\varepsilon = 0.01$ and for both $Ca = 0.01$ and $Ca = 1$. The $Ca = 1$ Stokes flow and (5.7) for $Ma = 1$ curves agree well. This indicates that $Ca = 1$ represents the high Ca limit at least to $k \sim 8$, and that $\varepsilon = 0.01$ is small enough so that the thin film limit applies. It follows, in particular, that the core's dynamics, which (cf. (4.10)) are not, in general, Stokes flows, do not affect the interface's stability to leading order. The $Ca = 0.01$ curve diverges from the others for $k > 2$; this indicates the short-wave stabilization of a finite capillary force, which scales $\sim k^4/Ca$ and dominates at high k. HF's Appendix D is somewhat comparable in spirit, but unlike (5.6), it is restricted to Stokes flow and unlike our Appendix, it and FH are concerned with a planar geometry, where circumferential curvature does not arise. Note that all of our cases, as well as theirs, yield quadratics for the growth rate as a result of two $\partial/\partial t$ terms in (2.11)–(2.12).

Figure 5 illustrates the mechanism of this instability, which derives mathematically from the term $(-2/m)\eta_z$ in (5.6*b*), for the plus mode of (5.7). (FH simply note that G and η being out of phase – their η troughs correspond to our η crests and thus their notion of in and out of phase are opposite to ours – in the eigenfunction yields destabilizing tractions.) This term expresses the correction to the advection of the unperturbed surfactant concentration by the change in the base flow's interfacial velocity owing to the displacement of the interface. That is, the displaced interfacial velocity feels the gradient in the r-direction of the undisturbed base flow velocity. The

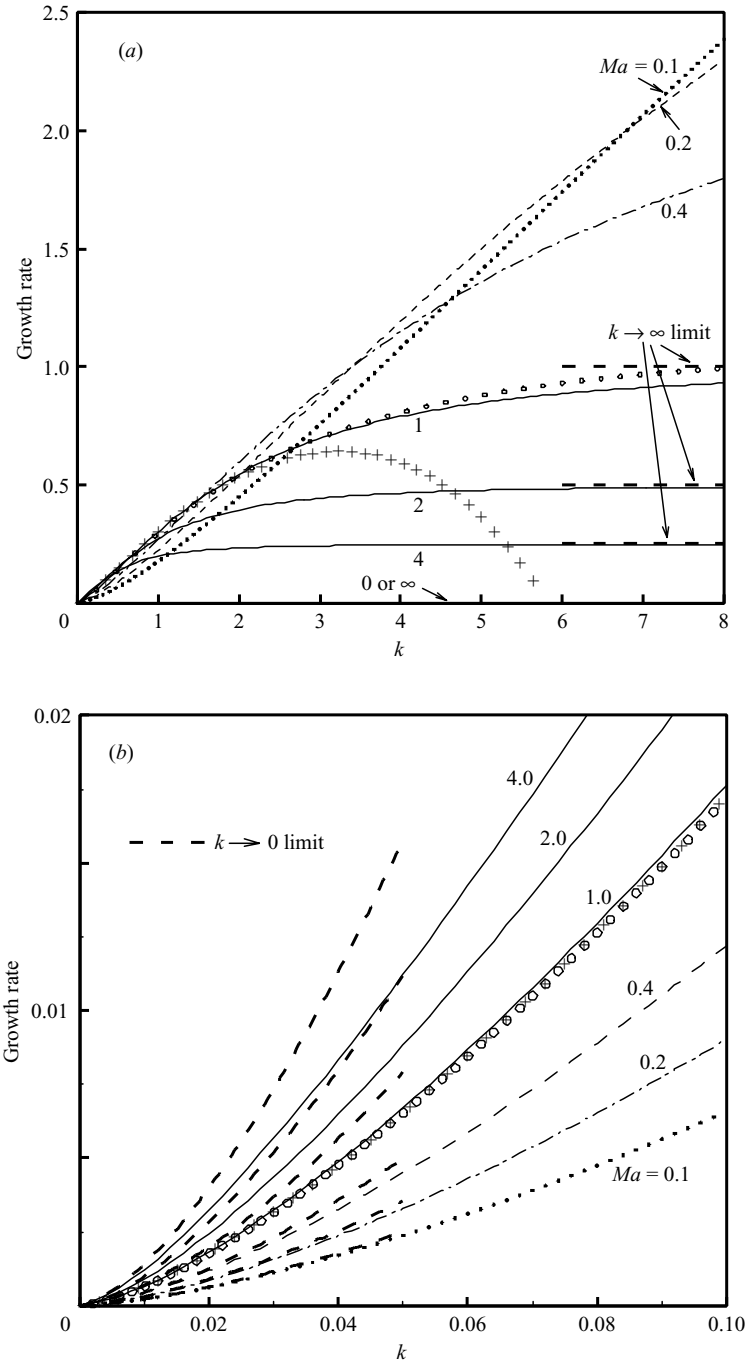

FIGURE 4. The weak tension limit for $m = 1$. (*a*) The growth rates *vs.* k for different Ma. (*b*) The same growth rates as in (*a*) in the long-wave regime together with their long-wave limits. The figures compare these results with the growth rate curves derived from the Stokes flow analysis in the Appendix, for $\varepsilon = 0.01$ and $Ma = 1$ for both $Ca = 0.01$ (symbol +) and $Ca = 1$ (symbol ○). The agreement is very good except for the $k > 2$ portion of the $Ca = 0.01$ curve, because capillary forces deriving from the interface's longitudinal curvature, acting as $-k^4/Ca$, are no longer negligible for short waves.

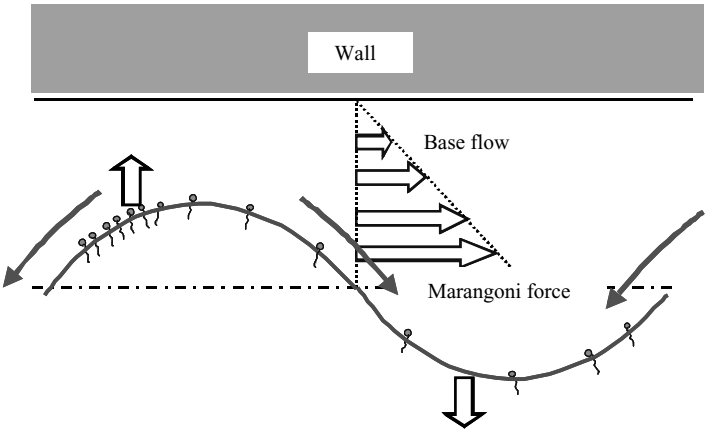

FIGURE 5. An illustration of the mechanism for how the base shear flow reorganizes the insoluble surfactants so that the resulting Marangoni forces can linearly destabilize the system. The crest of the disturbed interface feels a lower base velocity than does the trough. This sweeps surfactant from the trough to the crest region. The Marangoni term in (5.6*b*), reflecting the sweeping of surfactant attributable to the perturbation in the axial velocity caused by the displacement of the interface, acts diffusively to relieve the peak concentration at the interface crest, thereby introducing a phase-shift between the interface and surfactant profiles. The rearranged surfactant profile induces Marangoni forces that pull the interface from the surfactant maxima towards its minima, thereby further draining the film near the crest.

crest of the perturbed interface experiences a lower interfacial velocity than the trough and this sweeps surfactant from the trough region towards the crest. The Marangoni term in (5.6*b*) has a diffusive form and represents advection from regions of high towards regions of low surface concentration. The superposition of these two effects shifts the minimum velocity/maximum Γ to the left of the crest and the maximum velocity/minimum Γ to the left of the trough, thereby introducing a small phase lag between Γ and η. (The ratio $\hat{G}/\hat{\eta}$ gives a phase difference of $\pi/4$ as $k \to 0$, decreasing to 0 as $k \to \infty$.) Marangoni forces pull the interface from the Γ maxima towards its minima. This is reflected in the Marangoni term in the interface equation (5.6*a*) that causes the perturbation to grow by raising the interface position at the Γ_{zz} minima and decreasing it at the Γ_{zz} maxima, which are close to the Γ maxima and minima, respectively. (Note that deleting the Marangoni term in (5.6*a*) removes the k^3 term, and thus the instability, in (5.7).) A travelling reference frame removes the second terms in both of (5.6); thus they do not contribute to instability.

The minus mode corresponds to an eigenfunction where the perturbations to the surfactant concentration and interfacial position are closer to being out of phase ($-\pi/4$ for $k \to 0$, decreasing to $-\pi$ as $k \to \infty$). Thus the Marangoni contribution to (5.6*a*) tends to relieve the η disturbance and the gradient in the base flow tends to relieve the perturbation to the surfactant distribution.

We now explain the features of figure 4 in terms of this + mechanism. Figure 4 shows that the system is unstable for all $k \leqslant O(1)$, and the growth rate increases as k increases for fixed *Ma*. In the long wave limit (figure 4*b*), the growth rate increases with increasing *Ma*. For fixed *Ma*, i.e. fixed amount of surfactant, $k \to 0$ increases the separation between the higher Γ crests and the lower Γ troughs, thereby decreasing the Γ-gradient, and thus the driving force for the instability. For sufficiently long waves, increasing *Ma* at fixed k increases the total amount of surfactant at fixed

perturbation wavelength, and thus increases the gradients/driving forces. Both trends are consistent with the small k limit (5.8) of (5.7) which is similar to FH's table 1:

$$s \to -\frac{2\mathrm{i}}{m}k \pm \frac{\mathrm{i}^{1/2}}{m}Ma^{1/2}k^{3/2} \text{ as } k \to 0. \tag{5.8}$$

$Ma = 0$ is simply a neutral state; in the zero surface-tension limit when $Ma = 0$, neither capillary nor Marangoni forces contribute, and there is nothing to destabilize the system.

Increasing k (while keeping $k \ll \varepsilon^{-1}$ to maintain the validity of the lubrication treatment of the annulus) decreases the distances between crests and troughs. At fixed Ma (fixed total surfactant), this increases the surfactant gradients, and thus the driving force, thereby leading to a monotonic increase of the growth rate with k. This effect is tempered at large k by the fact that, at a fixed Ma, interfacial stiffness prevents the buildup of unbounded gradients, and so the effect saturates. (HF's figure 17a shows that the growth rate goes through a maximum for zero base-state tension near our $k \sim 1/\varepsilon$, which is beyond the scope of our theory. However, in the absence of surface tension and at zero Re, it is unclear physically what is causing this stabilization.) Since we are in the large Ca limit, increasing an already large Ma increases El, i.e. leads to a tangential stiffening of the interface, and thus to a decrease in the growth rate. This trend (figure 4a) is opposite to that observed in the $k \to 0$ limit above. In fact, for $kMa \gg 1$, (5.7) becomes

$$s = -\frac{\mathrm{i}}{m}k + \frac{1}{mMa} - \frac{2\mathrm{i}}{mMa^2k} - \frac{5}{mMa^3k^2} + k^2MaO(kMa)^{-5}. \tag{5.9}$$

From (5.9) it is clear that, at large kMa, the limiting value of the growth rate is $1/(mMa)$, which goes to zero as the interface becomes stiff, i.e. as $Ma \to \infty$. HF exhibits this numerically for $\sigma \neq 0$, as does our figure 4(a). That this is a large kMa limit, implies that the value of k for which, (5.9) represents (5.7) well, decreases inversely as Ma goes up. This explains why the curves in figure 4 show that, the higher the value of Ma, the faster (i.e. the lower the k value) the corresponding curve approaches its large k limit. In addition, the wave speed, $1/m$, in the $Ma \to \infty$ limit is independent of Ma and equal to $\frac{1}{2}$ of the base flow's interfacial velocity, $2/m$. As $Ma \to \infty$, the interface becomes tangentially stiff and retards the induced velocity (that stretches the interface) relative to the base flow; unlike in the no-flow case, the interface still convects.

As we shall see in § 5.4, when both Marangoni and capillary forces are present at leading order, we should expect flow-induced Marangoni destabilization at short waves to shift the marginal wavenumber of pure capillarity to shorter waves.

5.3. *Large and small Marangoni numbers*

As $Ma \to 0$ (i.e. for $Ma \ll \varepsilon^0$), (4.9a) reduces to

$$\eta_\tau + \frac{2}{m}\eta_z + \frac{1}{3mCa_0}(\eta_{zz} + \eta_{zzzz}) = 0. \tag{5.10}$$

The corresponding expression for s is

$$s = -\frac{2}{m}\mathrm{i}k + \frac{1}{3mCa_0}k^2(1 - k^2). \tag{5.11}$$

This is consistent with Georgiou *et al.*'s (1992) clean interface result.

A procedure similar to § 5.1 for the tangentially stiff limit, $Ma \to \infty$, suggests rescaling $G = \tilde{G}/Ma$, $\tilde{G} = O(1)$ in (4.9):

$$\eta_\tau + \frac{2}{m}\eta_z + \frac{1}{3mCa_0}(\eta_{zz} + \eta_{zzzz}) + \frac{1}{2m}\tilde{G}_{zz} = 0, \tag{5.12a}$$

$$-\frac{2}{m}\eta_z - \frac{1}{2mCa_0}(\eta_{zz} + \eta_{zzzz}) - \frac{1}{m}\tilde{G}_{zz} + O(Ma^{-1}) = 0. \tag{5.12b}$$

Eliminating $\tilde{G}_{zz}$ in (5.12*a*) yields for η and s:

$$\eta_\tau + \frac{1}{m}\eta_z + \frac{1}{12mCa_0}(\eta_{zz} + \eta_{zzzz}) = 0, \tag{5.13}$$

$$s = -\frac{1}{m}\mathrm{i}k + \frac{1}{12mCa_0}k^2(1 - k^2). \tag{5.14}$$

We also arrive at (5.14) by solving for s in (4.9) and taking the limit $Ma \to \infty$. The growth rate is again $1/4$ of that for the clean interface case, as in the tangentially stiff limit, (5.4), of the no-flow ($Ca_0 \to 0$) case. Yet the wave speed is half of the base flow's interfacial speed, as in the weak tension ($Ca_0 \to \infty$) case. Note that solving the disturbed film flow for a stiff-interface condition moving at the base flow's interfacial velocity leads to the correct growth rate, but with a wave speed of $(2/m)\eta_z$ instead of $(1/m)\eta_z$. This reduced s_i (the imaginary part of s) is consistent with the Marangoni instability mechanism's interfacial stretching. Marangoni forces resist this stretch, thereby slowing the wave speed; in the high Ma limit this retardation is maximum.

5.4. *General case*

We now apply normal mode analysis to the more general (4.9) and solve for s, yielding

$$s = -\frac{2}{m}\mathrm{i}k + \tfrac{1}{2}[-b(k) \pm \sqrt{b(k)^2 - 4c(k)}], \tag{5.15}$$

where

$$b(k) = \frac{Ma}{m}k^2 - \frac{1}{3mCa_0}k^2(1 - k^2), \quad c(k) = -\frac{Ma}{2m}k^2\left[\frac{2}{m}\mathrm{i}k + \frac{1}{6mCa_0}k^2(1 - k^2)\right].$$

Some formal limits are as follows. As $Ma \to 0$, (5.15) reduces to (5.11) for the clean interface. In the limit $Ma \to \infty$, (5.15) also reduces to (5.14), both consistent with the earlier analysis. As $Ca_0 \to 0$, replacing $Ma = El_0/Ca_0$ leads to (5.2). In the limit $Ca_0 \to \infty$, (5.15) again reduces to (5.7). This therefore is a unified framework for all of the above limiting cases.

Having physically analysed the no base flow (§ 5.1) and zero capillarity (§ 5.2) limits, we can now understand how capillary and Marangoni forces act together in the presence of a base flow. Figure 6 shows the growth rate *vs.* k curves for different Ma at a fixed $Ca_0 = 1$, again, only for the more dangerous mode corresponding to the + in (5.15). They also show the Stokes flow calculation for $\varepsilon = 0.01$ and $Ca = 10^{-4}$, i.e. $Ca_0 = 1$, and $Ma = 1$. The agreement is excellent, since ε is small enough to be in the thin-film regime where the core does not influence the interface dynamics (but, unlike figure 4, we are clearly *not* in the zero tension limit). At $Ma = 0$, we have the Georgiou *et al.* (1992) limit of clean interface capillarity in a CAF. For small kMa (corresponding, in figure 6(*a*), to $Ma \lesssim 1$ and, in figure 6(*b*) for moderate k, to the lowest readable values of k), the growth rate and the marginal wavenumber increase as Ma increases. (The $k \to 0$ limit of (5.15) is still (5.8), suggesting that Marangoni

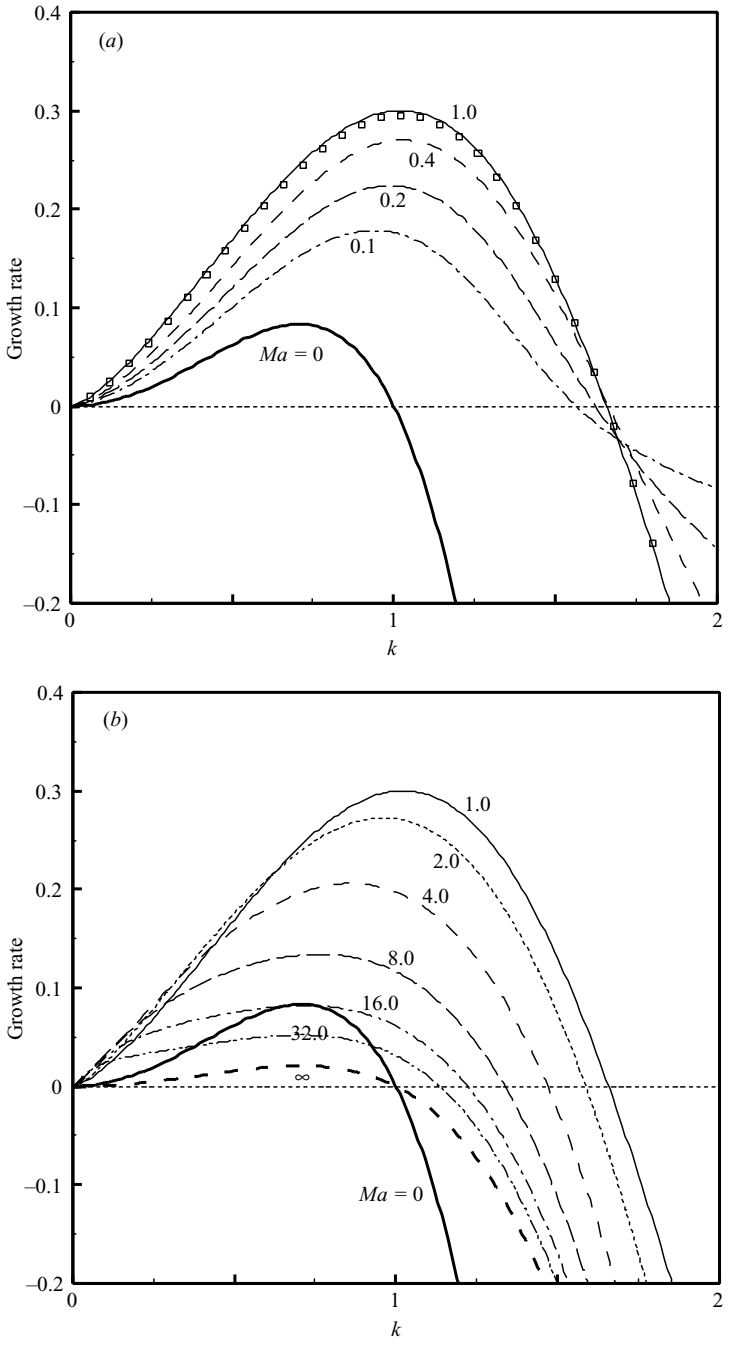

FIGURE 6. The growth rates *vs.* k for different Ma for the general case where both capillary and Marangoni forces are important and where the base flow is not negligible. In the figure, $Ca_0 = 1$ and $m = 1$. The figure compares these curves with the growth rate curve derived from the Stokes flow analysis for $\varepsilon = 0.01$, $Ma = 1$ and $Ca = 0.0001$ (symbol □). The agreement is excellent.

forces dominate capillarity for very long waves at fixed k.) Hence, at small kMa, increasing Ma at fixed k puts surfactant on a nearly clean interface; increasing k at fixed Ma decreases the distance between surfactant maxima. Each of these effects

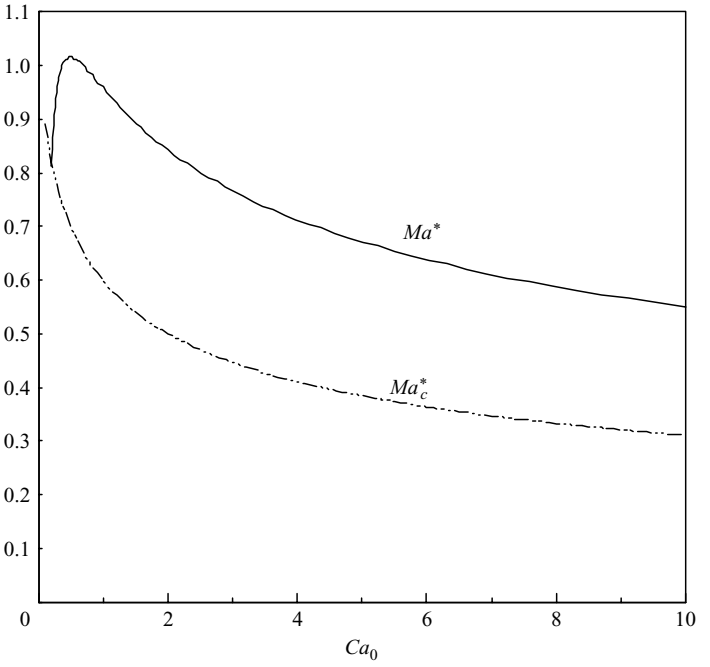

FIGURE 7. Ma^* and Ma_c^*, the Marangoni numbers at which the growth rate and the marginal wavenumber, respectively, begin to decrease with increasing Ma, as functions of Ca_0. Note that Ma_c^* decrease monotonically with Ca_0, while Ma^* goes through a maximum close to $Ca_0 = 0.5$ before decaying.

turns on and strengthens the destabilizing Marangoni forces of figures 4, raising the growth rate. Since this affects all wavenumber disturbances, k_c increases from its capillary value of one (shorter waves become linearly unstable) as kMa increases for small kMa. However, k_c does not diverge because capillary forces strongly stabilize the longitudinal curvature of short waves.

On the other hand, for large kMa, the Marangoni forces become weaker with further increase in Ma since, at such high surfactant concentrations, additional surfactant makes it harder for the flow to stretch the interfaces to create interfacial surfactant gradients. The result is a rapid lowering of the Marangoni-derived (figure 4*a*) and the overall growth (figure 6*b*), and a concomitant lowering of k_c in figure 6(*b*). For $Ma \to \infty$, this Marangoni effect disappears as $(mMa)^{-1}$ for all k (see figure 4*a* and (5.9)), and we recover the slowest growth of the tangentially stiff capillarity limit (5.14). The growth rate again becomes 1/4 that of the clean interface, k_c returns to one and, as noted in § 5.2, the wave speed becomes half the interfacial velocity. (For a planar flow, HF also find a growth rate maximum with Ma, but have a zero $Ma \to \infty$ limit.) The values Ma^* and Ma_c^* at which the growth rate and marginal wavenumber cease to increase with increasing Ma differ and each depends on Ca_0. Figure 7 shows these dependences.

For small Ca_0, the base flow is weak (i.e. $\mu_1 W_0 \ll \sigma_0^*$), and capillary forces dominate the stability picture. As already shown in § 5.1 for the $Ca_0 \to 0$ limit, increasing Ma just slows down the growth rate and so Ma^* is zero for $Ca_0 \to 0$. For some small Ca_0 (not shown), the maximum growth rate decreases, increases, then decreases again as Ma increases from 0, but the maximum growth rate is still at $Ma = 0$ because the

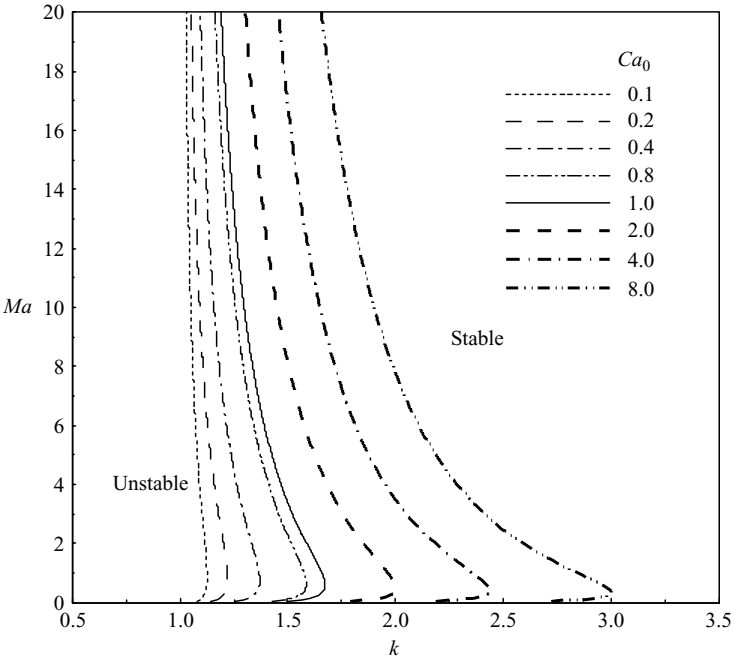

FIGURE 8. Neutral stability curves of Ma *vs.* k for different Ca_0 for $m = 1$. The unstable region becomes wider, i.e. k_c increases, as Ca_0 increases at fixed Ma, i.e. as viscous forces sweep more surfactant along the interface at fixed surfactant concentration and surface tension. For large Ma, as Ma increases at fixed Ca_0, the interface fills with surfactant, no longer allowing surfactant gradients to arise, and the critical wavenumber returns to its non-dimensional capillary value of 1.

Marangoni instability is weak in this limit. Thus, $Ma^* = 0$ for the small Ca_0 limit. Increasing Ca_0 strengthens the influence of the base flow so that it can rearrange the surfactant, i.e. it turns on the destabilizing Marangoni forces, and thus increases Ma^*. As figure 7 shows, upon increasing Ca_0, Ma^* rapidly reaches a maximum (~ 1) at $Ca_0 \sim 0.5$ and then slowly decreases for larger Ca_0. HF's planar case (figure 9 – for $m = 0$ (in our notation; their m is the inverse of ours) to order ε^0) has Ma^* monotonically decreasing with Ca_0.

Figure 8 shows neutral curves of Ma *vs.* k for different Ca_0. For each value of Ca_0, increasing Ma from zero first widens the instability region (i.e. increases k_c in figure 6), and then narrows it. For increasing Ca_0, the instability regime expands since, at each Ma, increasing Ca_0 corresponds to decreasing surface tension forces relative to Marangoni forces, thereby magnifying the effect. For large Ma, all curves converge to the marginal wavenumber $k_c = 1$ because the interface becomes tangentially stiff (cf. (5.14)). In contrast to Ma^*, Ma_c^*, where k_c in figure 6(b) begins to fall, appears (figure 7) to decrease monotonically with increasing Ca_0 and has only a weak Ca_0 dependence.

6. Application to oil recovery and to oil recovery in rock pores and to the lung

As a typical example of a liquid–liquid displacement, consider an oil film of $\mu_2 = 10\,\text{cP}$ surrounding a water slug ($\mu_1 = 1\,\text{cP}$) with an interfacial tension of $10\,\text{dyn cm}^{-1}$ in a $200\,\mu\text{m}$ diameter tube (whose circumference is $628\,\mu\text{m}$). A typical slug velocity is about $1\,\text{cm s}^{-1}$. The surface concentration of an insoluble surfactant can range from

10^{-12} to 10^{-10} mol cm^{-2}. Consider a film thickness of 10 μm, or $\varepsilon = 0.1$. These numbers give $Re_1 \sim 1$, $Ca \sim 10^{-2}$, $m = 10$ and Ma ranges from 2.5 to 250, which is in the range of the analysis in § 5.4. With these parameters, the zero-surfactant-activity limit, i.e. $Ma = 0$ in figure 6 or $El_0 = 0$ in figure 2, gives a maximum growth rate of 0.05 min^{-1}, i.e. about a 14 min doubling time. The corresponding wavelength is 888 μm and the wave speed is 200 μm s^{-1}. $k_{max} = 1/\sqrt{2}$ and the marginal wavenumber is $k_c = 1$. For a moderate $Ma \sim 2.5$, figure 6(b) predicts a maximum growth rate of 0.15 min^{-1}. This growth rate is three times the zero-surfactant-activity case. The corresponding wavelength is 560 μm and the wave speed is 35 μm s^{-1} for $k_{max} \sim 0.94$. That is, the wave speed is reduced by a factor of about 6 compared with the zero-surfactant-activity case because the interface is less mobile. The marginal wavelength shortens to 443 μm for $k_c \sim 1.42$. On the other hand, for large $Ma \sim 250$, figure 6(b) predicts the maximum growth rate should be $\sim 1/4$ of that of the zero-surfactant-activity case, or 0.0125 min^{-1}. Thus, surfactant makes the system more stable than the surfactant-free case. The corresponding k_{max} remains almost unchanged, but the wave speed is reduced to 100 μm s^{-1}, half that of the zero-surfactant-activity case.

Consider now the liquid lining in the small airways of the lung. The liquid lining in the lungs is comprised of two layers, a low-viscosity watery liquid (Sleigh 1991; Yeates 1991), called the periciliary sol, surrounding the cilia, covered by a viscoelastic mucous layer. The periciliary layer is considered by physiologists to be Newtonian (Yeates 1991), and its low viscosity allows the cilia to develop rapid powerful strokes without being restrained by the thick mucus. Mucus-secreting cells are in abundance in the bronchi, but are mostly replaced by the non-mucus-secreting Clara cells in the smaller bronchioles (Widdicombe 2002). As a result, Sleigh (1991) notes that the mucous layer is likely to be extremely thin, or even discontinuous, in the bronchioles. As such, it is probably not unreasonable in a first model – and until more is known about the thickness, continuity and importance of the mucous layer in the bronchioles, as opposed to in the bronchi – to consider the fluid lining the bronchioles as being Newtonian, with the surfactant exerting a strong influence on its interfacial properties, and to ignore the mucus. Naturally, should it turn out that there is indeed a continuous mucous layer in the bronchioles, the applicability of this theory – in particular the control of the surface properties by (2.5) and (2.12) – to bronchioles would be put into question.

Let us move to an example of a generation 18 respiratory bronchiole, which has a diameter of about 400 μm. The core fluid is air ($\mu_1 = 0.02$ cP). A liquid layer of thickness 5 μm ($\varepsilon = 0.025$) and $\mu_2 = 1$ cP, similar to water, coats these small airways. The air–liquid surface tension is 10 dyn cm^{-1} in the presence of surfactant. The velocity of the air in this small airway is 0.4 cm s^{-1}. These give $Re_1 \sim 5 \times 10^{-2}$, $Ca \sim 10^{-5}$ and $m = 50$; thus Ca is clearly small (say, $< O(\varepsilon^2)$), and we are in the zero flow limit of § 5.1. The zero-surfactant-activity limit (figure 2) has a maximum growth rate of 0.8 min^{-1}, i.e. about a 0.9 min doubling time. Since viscous forces from the base flow are negligible relative to surface tension forces, the Marangoni instability is absent, surfactant tends to stabilize the system, and $k_c \sim 1$. For large Ma, the maximum growth (figure 2) is reduced to 0.2 min^{-1} (1/4 that of the zero-surfactant-activity case).

It is widely believed that lowering the tension of the interface between the air and the liquid lining of the lung airways delays airway closure to scales longer than the breathing cycle. This prevents closure, and is the primary role of pulmonary surfactant (Avery & Mead 1959; Macklem, Proctor & Hogg 1970). It is well known (Chandrasekhar 1961) and evident from (5.15) that lowering σ_0^* increases the time scale for the capillary instability. Even though both of these are linear analyses, and

thus only apply to small deviations from the cylindrical shape, it is well established that the linear theory for cylindrical interfaces, as in jets, has a surprisingly long reach, with the linear growth rate providing unusually good estimates of the collapse times of such interfaces (Bogy 1979). Slowing the unstable growth by the inclusion of a surfactant clearly does this in the no-flow or strong-tension ($Ca \ll \varepsilon^2$) limit, which, as figure 2 demonstrates, applies to the bronchioles. However, for larger Ca, figure 6 demonstrates that the effect of adding surfactant is more complex, since the flow can strongly interact with the surfactant distribution.

For liquid plug formation, as in surfactant replacement therapy, consider a slightly larger airway, say the tenth generation, having a 0.13 cm inner diameter. The core fluid is still air (0.02 cP) and the annular film has properties similar to water (1 cP). The film thickness is about 10 % of the airway diameter, i.e. $\varepsilon = 0.1$. The air–liquid surface tension is 20 dyn cm^{-1} when exogenous surfactants are present. For a breathing rate of 30 min^{-1} and a tidal volume of 500 ml, the average air speed in this airway is about 17 cm s^{-1}. These conditions give $Re_1 \sim 2 \times 10$ (*not* Stokes flow), $Ca \sim 10^{-3}$ and $m = 50$, which is the regime of $Ca \sim \varepsilon^2$ or less. If a surfactant is selected or dosed to give $Ma \sim 1$, then the maximum growth rate (figures 6) is 2.2 min^{-1}, or about 6 times the clean-interface value. Thus the presence of surfactant could promote the formation of liquid plugs. The corresponding k_{max} is 1.5. In this case, if a liquid plug forms and if we can estimate its size as half the wavelength corresponding to k_{max}, then the predicted length of a liquid plug is ~ 0.94 cm. This length is shorter than (2/3 of) the airway's periphery. However, such a liquid plug's mobility ~ 0.12 cm s^{-1} (estimated via s_i) is slower than the clean-interface value (0.4 cm s^{-1}).

7. Concluding remarks

We use scaling and asymptotic analysis to investigate the effects of insoluble surfactants on the linear stability of a core–annular flow. The novelty here is the effect of a base shear flow on the interplay of capillary and Marangoni forces. We also allow $O(1)Re_1$. In the thin-film limit, we derive a set of film evolution equations that couples the perturbations to the interfacial position and to the surfactant concentration and governs the system's linear stability. The core dynamics are slaved to those of the film. Our theory provides a unified theoretical basis for the instability mechanisms in three different regimes: (i) the strong tension/ no base flow limit, (ii) the weak tension/ strong base flow limit, and (iii) the moderately strong tension case. In each regime, we explain how the base flow affects the distribution of insoluble surfactants and how the resulting Marangoni and, except in (ii), capillary forces determine the system's linear stability. In different regimes, adding surfactants to a clean interface can make it more or less stable.

Without a base flow, Marangoni forces deriving from the perturbed distribution of insoluble surfactants slow down the effects of capillary forces, both for perturbations with $k > 1$ that they usually stabilize and those with $k < 1$ that they usually destabilize. For weak tension forces, a base flow rearranges the surfactant at an interface with a perturbed shape, generating Marangoni forces that destabilize the system to disturbances of all k ($\ll 1/\varepsilon$). The growth rate increases monotonically with k, but asymptotes at large kMa to a value that goes as $1/mMa$. Thus, the system is unstable to disturbances of any wavelength unless capillary forces, that strongly resist the longitudinal curvature introduced by short waves, participate and thereby stabilize them. When a base flow is present and capillary forces are in play, Marangoni forces try to destabilize all wavelength disturbances; they widen the unstable region by shifting the

marginal k_c to shorter waves than for a clean interface. For a large interfacial elasticity, the interface becomes tangentially stiff and, in the absence of a base flow, immobile. This results in a capillarity-driven growth rate lower than that (in fact, 1/4) of the clean interface and the non-dimensionalized marginal wavenumber returns to 1.

This analysis suggests a number of extensions. First, one could consider soluble, rather than insoluble surfactants. At low and moderate tensions, the surfactant concentration gradient along the interface is expected to be less than in the insoluble case, and therefore the resulting Marangoni destabilization should be weaker. A detailed study of this problem depends on the sorption kinetics and on the bulk surfactant transport in both the core and the film. Second, the present theory is in a parameter regime where the core flow does not contribute to the interfacial stability. Different scalings (e.g. a weaker surface tension) would couple the core dynamics to the Marangoni stresses at the interface and thus to the interface evolution. In Papageorgiou *et al.* (1990) and Georgiou *et al.* (1992), both surfactant-free studies, a less strong surface tension ($Ca \sim \varepsilon$) couples the core to the interface problem (via the tangential stress balance) when the two fluids have different viscosities. There, the less viscous annulus case ($m < 1$) can result in a linear stability window in Reynolds-number space. Since, as we have seen, Marangoni forces can strongly destabilize, it would be interesting to see how surfactants alter this stability window.

Another direction is to extend the present linear theory into the weakly nonlinear regime. Earlier studies (Frenkel *et al.* 1987; Papageorgiou *et al.* 1990) have shown that the capillary instability can be saturated in the weakly nonlinear regime due to the Kuramoto–Sivashinsky nonlinearity. This saturation arises in the leading-order problem in the parameter regime of moderately strong tensions $\varepsilon^2 \ll Ca \lesssim \varepsilon$. As we have seen, in the presence of a non-trivial base flow, the induced Marangoni forces destabilize for all wavelengths $\gg O(\varepsilon)$. In particular, for $k > 1$ but $k = O(1)$, Marangoni forces destabilize and capillary forces weakly stabilize. Thus, it would seem that Marangoni forces would destabilize these waves, and nonlinear effects would steepen them to a point where short-wave capillary stabilization would compete with Marangoni destabilization. It would be interesting to see whether this competition would cause the waves to first saturate or become $O(\varepsilon)$. The detailed result should depend on the relative scalings of ε, Ma, Ca, and the sizes of both interface and surfactant concentration perturbations.

We thank the donors of the Petroleum Research Fund (27403-AC9 to DSR) and the National Science Council of Taiwan (NSC92-2218-E006-057 to HHW) for supporting this work.

Appendix. The full, unscaled linear stability equations in the $Re \to 0$ limit

We begin by introducing a perturbed streamfunction Ψ_i for each fluid $i = 1, 2$,

$$w_i = \frac{1}{r}\frac{\partial \Psi_i}{\partial r}, \quad u_i = -\frac{1}{r}\frac{\partial \Psi_i}{\partial z}\,. \tag{A 1}$$

We rewrite the Stokes equations and the linearized boundary conditions for the perturbed quantities in terms of Ψ_i, η and G, and apply the normal modes

$$(\Psi_i, \eta, G) = (\hat{\psi}_i, \hat{\eta}, \hat{G}) \exp(\mathrm{i}kz + st) \tag{A 2}$$

to derive the governing equations for perturbed fluid motions as

$$\mathrm{D}(\mathrm{D}\hat{\psi}_i) = 0\,, \tag{A 3}$$

where

$$\mathrm{D} := \frac{\mathrm{d}^2}{\mathrm{d}r^2} - \frac{1}{r}\frac{\mathrm{d}}{\mathrm{d}r} - k^2.$$

The linearized boundary conditions, in terms of $\left(\hat{\psi}_i, \hat{\eta}, \hat{G}\right)$, are:

$$\frac{\hat{\psi}_2}{r} = 0, \frac{1}{r}\hat{\psi}_{2r} = 0 \quad \text{at } r = a, \tag{A 4}$$

$$\frac{\hat{\psi}_1}{r} < \infty, \frac{1}{r}\hat{\psi}_{1r} < \infty \quad \text{at } r = 0, \tag{A 5}$$

$$\frac{1}{r}(\hat{\psi}_{1_r} - \hat{\psi}_{2_r}) - (\overline{w}_r - \overline{W}_r)\hat{\eta} = 0 \quad \text{at } r = 1, \tag{A 6}$$

$$\frac{1}{r}(\hat{\psi}_1 - \hat{\psi}_2) = 0 \quad \text{at } r = 1, \tag{A 7}$$

$$[\mathrm{D}\hat{\psi}_1 + 2k^2\hat{\psi}_1] - m[\mathrm{D}\hat{\psi}_2 + 2k^2\hat{\psi}_2] + \mathrm{i}kMa\hat{G} = 0 \quad \text{at } r = 1, \tag{A 8}$$

$$\frac{m}{\mathrm{i}kr}[\mathrm{D}\hat{\psi}_2]_r + 2\mathrm{i}km\left[\frac{1}{r}\hat{\psi}_2\right]_r - \frac{1}{\mathrm{i}kr}\left[\mathrm{D}\hat{\psi}_1\right]_r - 2\mathrm{i}k\left[\frac{1}{r}\hat{\psi}_1\right]_r - \frac{1}{Ca}(k^2 - 1)\hat{\eta} - \frac{El}{Ca}\hat{G} = 0 \quad \text{at } r = 1, \tag{A 9}$$

$$-\frac{\mathrm{i}k}{r}\hat{\psi}_2 - (s + \mathrm{i}k\overline{w})\,\hat{\eta} = 0 \quad \text{at } r = 1, \tag{A 10}$$

$$(s + \mathrm{i}k\overline{w})\,\hat{G} + \mathrm{i}k\overline{w}_r\hat{\eta} + \frac{\mathrm{i}k}{r}\hat{\psi}_2 = 0 \quad \text{at } r = 1. \tag{A 11}$$

The solutions for the core and the annulus are, respectively,

$$\hat{\psi}_1 = A_1 r I_1(kr) + B_1 r^2 I_0(kr), \tag{A 12}$$

$$\hat{\psi}_2 = A_2 r I_1(kr) + B_2 r^2 I_0(kr) + C_2 r K_1(kr) + D_2 r^2 K_0(kr). \tag{A 13}$$

I_n and K_n are modified Bessel functions of the first and second kinds, respectively, of order n.

Substituting the solutions (A 12) and (A 13) into the boundary conditions (A 4)–(A 11), we arrive, with some manipulations, at the (8×8) system of equations

$$\boldsymbol{M} \cdot \boldsymbol{x} = 0, \tag{A 14}$$

where $\boldsymbol{x}$ is the vector of unknown coefficients $\boldsymbol{x} = [A_1, B_1, A_2, B_2, C_2, D_2, \hat{\eta}, \hat{G}]^t$, and the matrix $\boldsymbol{M} \equiv M_{ij}$ has the following components:

$$M_{11} = 0, \quad M_{12} = 0, \quad M_{13} = kaI_0(ka), \quad M_{14} = 2aI_0(ka) + ka^2 I_1(ka),$$
$$M_{15} = -kaK_0(ka), \quad M_{16} = 2aK_0(ka) - ka^2 K_1(ka), \quad M_{17} = 0, \quad M_{18} = 0,$$
$$M_{21} = 0, \quad M_{22} = 0, \quad M_{23} = kaI_1(ka), \quad M_{24} = a^2 I_0(ka), \quad M_{25} = aK_1(ka),$$
$$M_{26} = a^2 K_0(ka), \quad M_{27} = 0, \quad M_{28} = 0, \quad M_{31} = kI_0(k), \quad M_{32} = 2I_0(k) + kI_1(k),$$
$$M_{33} = -kI_0(k), \quad M_{34} = -2I_0(k) - kI_1(k), \quad M_{35} = kK_0(ka),$$
$$M_{36} = -2K_0(ka) + kK_1(ka), \quad M_{37} = -2(m-1)/(a^2 + m - 1), \quad M_{38} = 0,$$
$$M_{41} = \mathrm{i}kI_1(k), \quad M_{42} = \mathrm{i}kI_0(k), \quad M_{43} = 0, \quad M_{44} = 0, \quad M_{45} = 0, \quad M_{46} = 0,$$
$$M_{47} = s + \mathrm{i}k\overline{w}(r = 1), \quad M_{48} = 0, \quad M_{51} = 0, \quad M_{52} = 0, \quad M_{53} = \mathrm{i}kI_1(k),$$
$$M_{54} = \mathrm{i}kI_0(k), \quad M_{55} = \mathrm{i}kK_1(k), \quad M_{56} = \mathrm{i}kK_0(k), \quad M_{57} = s + \mathrm{i}k\overline{w}(r = 1),$$

$$M_{58}=0,\quad M_{61}=0,\quad M_{62}=I_1(k),\quad M_{63}=0,\quad M_{64}=-mI_1(k),\quad M_{65}=0,$$
$$M_{66}=mK_1(k),\quad M_{67}=\mathrm{i}(1-m)(s+\mathrm{i}k\overline{w}(r=1)),\quad M_{68}=\mathrm{i}Ma/2,$$
$$M_{71}=2\mathrm{i}k^2(m-1)I_0(k),\quad M_{72}=2\mathrm{i}k(2m-1)I_0(k)+2\mathrm{i}k^2(m-1)I_1(k),$$
$$M_{73}=0,\quad M_{74}=-2\mathrm{i}kmI_0(k),\quad M_{75}=0,\quad M_{76}=-2\mathrm{i}kmK_0(k),$$
$$M_{77}=2(m-1)(s+\mathrm{i}k\overline{w}(r=1))-4\mathrm{i}km(m-1)/(a^2+m-1)-(1-k^2)/Ca,$$
$$M_{78}=-Ma,\quad M_{81}=\mathrm{i}k^2I_0(k),\quad M_{82}=\mathrm{i}k(2I_0(k)+kI_1(k)),\quad M_{83}=0,\quad M_{84}=0,$$
$$M_{85}=0,\quad M_{86}=0,\quad M_{87}=-2\mathrm{i}km/(a^2+m-1),\quad M_{88}=s+\mathrm{i}k\overline{w}(r=1).$$

Setting the determinant of $\boldsymbol{M}$ to zero provides an equation for the complex growth rate s that reduces to a quadratic equation with complex coefficients. This formulation provides a simple way to solve for s numerically for any set of values for a, m, k, Ca and Ma.

REFERENCES

Avery, M. E. & Mead, J. 1959 Surface properties in relation to atelectasis and hyaline membrane disease. *AMA J. Dis. Child* **97**, 517–523.

Babadagli, T. 2003 Selection of proper enhanced oil recovery fluid for efficient matrix recovery in fractured oil reservoirs. *Colloid Surface* A **223**, 157–175.

Blyth, M. G. & Pozrikidis, C. 2004 Effect of surfactants on the stability of two-layer channel flow. *J. Fluid Mech.* **505**, 59–86.

Bogy, D. B. 1979 Drop formation in a circular liquid jet. *Annu. Rev. Fluid Mech.* **11**, 207–228.

Carroll, B. & Lucassen, J. 1974 Effect of surface dynamics on the process of droplet formation from supported and free liquid cylinders. *J. Chem. Soc. Faraday Trans.* **70**, 1228–1239.

Cassidy, K. J., Halpern, D., Ressler, B. G. & Grotberg, J. B. 1999 Surfactant effects in model airway closure experiments. *J. Appl. Physiol.* **87**, 415–427.

Chandrasekhar, S. 1961 *Hydrodynamics and Hydromagnetic Stability*. Dover.

Craster, R. V., Matar, O. K. & Papageorgiou, D. T. 2002 Pinchoff and satellite formation in surfactant covered viscous threads. *Phys. Fluids* **14**, 1364–1376.

Dijkstra, H. A. & Steen, P. H. 1991 Thermocapillary stabilization of the capillary breakup of an annular film of liquid. *J. Fluid Mech.* **229**, 205–228.

Espinosa, F. F. & Kamm, R. D. 1999 Bolus dispersal through the lungs in surfactant replacement therapy. *J. Appl. Physiol.* **86**, 391–410.

Frenkel, A. L., Babchin, A. J., Levich, B. G., Shlang, T. & Sivashinsky, G. I. 1987 Annular flows can keep unstable film from breakup: nonlinear saturation of capillary instability. *J. Colloid Interface Sci.* **115**, 225–233.

Frenkel, A. L. & Halpern, D. 2002 Stokes–flow instability due to interfacial surfactant. *Phys. Fluids* **14**, L45–L48.

Georgiou, E. C., Papageorgiou, D. T., Maldarelli, C. & Rumschitzki, D. S. 1992 An asymptotic theory for the linear stability of a core–annular flow in the thin annular limit. *J. Fluid Mech.* **243**, 653–677.

Goren, S. L. 1962 The instability of an annular thread of fluid. *J. Fluid Mech.* **12**, 309–319.

Goussis, D. A. & Kelly, R. E. 1991 Surface wave and thermocapillary instability in a liquid film-flow. *J. Fluid Mech.* **223**, 25–45.

Halpern, D. & Frenkel, A. L. 2003 Destabilization of a creeping flow by interfacial surfactant: linear theory extended to all wavenumbers. *J. Fluid Mech.* **485**, 191–220.

Halpern, D. & Grotberg, J. B. 1993 Surfactant effects on fluid–elastic instabilities of liquid-lined flexible tubes: a model of airway closure. *J. Biomech. Engng* **115**, 271–277.

Halpern, D., Jensen, O. E. & Grotberg, J. B. 1998 A theoretical study of surfactant and liquid delivery into the lung. *J. Appl. Physiol.* **85**, 333–352.

Hammond, P. S. 1983 Nonlinear adjustment of a thin annular film of viscous fluid surrounding a thread of another within a circular cylindrical pipe. *J. Fluid Mech.* **137**, 363–384.

Hansen, S. Peters, G. W. M. & Meijer, H. E. H. 1999 The effect of surfactant on the stability of a fluid filament embedded in a viscous fluid. *J. Fluid Mech.* **382**, 331–349.

Hickox, C. E. 1971 Instability due to viscosity and density stratification in axisymmetrical pipe flow. *Phys. Fluids* **14**, 251.

Ji, W. & Setterwall, F. 1994 On the instabilities of vertical falling liquid films in the presence of surface-active solute. *J. Fluid Mech.* **278**, 297–323.

Kerchman, V. 1995 Strongly nonlinear interfacial dynamics in core–annular flows. *J. Fluid Mech.* **290**, 131–166.

Kwak, S. & Pozrikidis, C. 2001 Effect of surfactants on the instability of a liquid thread or annular layer. Part I: Quiescent fluids. *Intl J. Multiphase Flow* **27**, 1–37.

Lin, S. P. 1970 Stabilizing effects of surface-active agents on a film flow. *AIChE J.* **16**, 375–379.

Macklem, P. T., Proctor, D. F. & Hogg, J. C. 1970 Stability of peripheral airways. *Respir. Physiol.* **8**, 191–203.

Otis, D. R., Johnson, J. M., Pedley, T. J. & Kamm, R. D. 1993 Role of pulmonary surfactant in airway closure: a computational study. *J. Appl. Physiol.* **75**, 1323–1333.

Papageorgiou, D. T., Maldarelli, C. & Rumschitzki, D. S. 1990 Nonlinear interfacial stability of core annular flows. *Phys. Fluids* A **2**, 340–352.

Park, C. W. & Homsy, G. M. 1984 Two-phase displacement in Hele-Shaw cells: theory. *J. Fluid Mech.* **141**, 257–287.

Porzrikidis, C. 2003 Effect of surfactants on film flow down a periodic wall. *J. Fluid Mech.* **496**, 105–127.

Preziosi, L., Chen, K. & Joseph, D. D. 1989 Lubricated pipelining: stability of core–annular flow. *J. Fluid Mech.* **201**, 323–356.

Rayleigh, L. 1879 On the capillary phenomena of jets. *Proc. R. Soc.* A **29**, 71.

Slattery, J. C. 1974 Interfacial effects in the entrapment and displacement of residual oil. *AIChE. J.* **20**, 1145–1154.

Sleigh, M. A. 1991 Mucus propulsion. *The Lung: Scientific Foundations* (ed. R. G. Crystal & J. B. West), chap. 3.1.4. Raven, New York.

Smith, M. K. 1990 The long wave instability in heat or cooled inclined liquid layers. *J. Fluid Mech.* **219**, 337–360.

Tomokita, S. 1935 On the instability of a cylindrical thread of a viscous liquid surrounded by another viscous liquid. *Proc. R. Soc.* A **150**, 322–337.

Waxman, A. M. 1984 Dynamics of a couple-stress fluid membrane. *Stud. Appl. Maths* **70**, 63.

Wei, H.-H. & Rumschitzki, D. S. 2002 The linear stability of a core-annular flow in an asymptotically corrugated tube. *J. Fluid Mech.* **466**, 113–147.

Whitaker, S. & Jones, L. O. 1966 Stability of falling liquid films. Effect of interface and interfacial mass transport. *AIChE. J.* **12**, 421–431.

Widdicombe, J. H. 2002 Regulation of the depth and composition of airway surface liquid. *J. Anat.* **201**, 313–318.

Wong, H., Rumschitzki, D. S. & Maldarelli, C. 1996 On the surfactant mass balance at a deforming fluid interface. *Phys. Fluids* **8**, 3203–3204.

Yeates, D. B. 1991 Mucus rheology. *The Lung: Scientific Foundations* (ed. R. G. Crystal & J. B. West), chap. 3.1.5. Raven, New York.

Yih, C.-S. 1967 Instability due to viscosity stratification. *J. Fluid Mech.* **27**, 337–352.